Diplomarbeit

Impact of Urban Area Growth on ASCAT Backscatter Time Series as Depicted by Sentinel-1

ausgeführt zum Zwecke der Erlangung des akademischen Grades

Diplom-Ingenieur

im Rahmen des Studiums

Geodäsie und Geoinformation

eingereicht von

Gabriel Stollhof
Matrikelnummer 01126459

ausgeführt an der Forschungsgruppe Fernerkundung
am Department für Geodäsie und Geoinformation
der Fakultät für Mathematik und Geoinformation an der technischen Universität Wien

Betreuung:
Betreuer: Univ.Prof. Dipl.-Ing. Dr.techn. Wolfgang Wagner
Mitwirkung: Dipl. Ing. Claudio Navacchi & Dipl. Ing. Sebastian Hahn

Wien, 29. März 2023 _____   _____

(Unterschrift Verfasser)   (Unterschrift Betreuer)

Declaration

I declare that I have written this thesis under the auspices of the Department of Geodesy and Geoinformation by myself without any help or assistance of others. External literature, which has used to clarify the content, or provided data sources for research are clearly cited and attributed. This work has not been presented to any other testing authority before.

Date: 29.03.2023

_____

(Gabriel Stollhof)

Abstract

Urban areas have a significant effect on different types of datasets collected by remote sensing sensor systems. This thesis reports the investigation of high-resolution datasets derived from the Sentinel-1 C-SAR instrument regarding the effects of urban growth and its influence on the data derived from the Advanced Scatterometer instrument of the MetOp satellite. Datasets of both sensor systems from five different regions were matched and analyzed regarding their correlation. From the Sentinel-1 datasets gradient maps were created which allowed a detailed analysis of fine-scale temporal changes regarding backscatter behaviour. Three of the five Sentinel-1 datasets were suitable for in-depth experiments, which resulted in the isolation of many different kinds of influences on the backscatter data including some kinds of urban growth. With these experiments and the used algorithms an exact quantification of the influence of urban growth on the datasets was not possible but a baseline for further development has been created.

Kurzfassung

Urbane Regionen haben aufgrund ihrer physikalischen Eigenschaften signifikanten Einfluss auf Fernerkundungsdaten. Die vorliegende Arbeit beschäftigt sich mit der Untersuchung des Rückstreuverhaltens in urbanen Gebieten und dessen Auswirkungen auf Datensätze des auf den MetOp Satelliten montierten Advanced Scatterometer Sensors mithilfe von hochauflösenden Daten des C-SAR Sensorsystems der Sentinel-1 Satellitenmission. Hierfür wurden in fünf unterschiedlichen Regionen die Datensätze beider Sensorsysteme zeitlich und räumlich angeglichen und ihre Korrelation berechnet. Drei der fünf Sentinel-1 Datensätze eigneten sich für tiefergehende Experimente, die die Eingrenzung vieler verschiedener Einflüsse auf das Rückstreuverhalten inklusive mehrerer Arten von urbanem Wachstum, ermöglichten. Die durchgeführten Experimente und die benutzten Algorithmen ermöglichten keine exakte Quantifizierung des Einflusses von urbanem Wachstum auf die Daten, jedoch war es möglich eine Ausgangsbasis für zukünftige Weiterentwicklungen zu erstellen.

Table of Contents

1 Introduction

1.1 Motivation

Microwave remote sensing data is widely utilized for a vast variety of use cases nowadays. The introduction of high resolution sensor systems and the start of many new satellite missions raised the number and quality of available datasets hugely in the past decades. One difficulty in processing this data and getting a high quality product are unwanted influences, which distort the data. Pinpointing these influences is harder when the spatial resolution of the datasets is low. Especially in urban areas the datasets derived from measurements from the Advanced Scatterometer (ASCAT) show a trend, which is deviating from the trends of the surrounding, lesser populated, areas. This directly affects products derived from the ASCAT datasets as for example soil moisture models. To verify that urban growth is a driving factor behind these trends, the extraction of small scale influences and the evaluation of their impact using high resolution datasets from a modern satellite system (Sentinel-1) are chosen as methods in this thesis. The idea behind this approach is that, when the ASCAT and Sentinel-1 datasets correlate on a big scale level, the investigation of the Sentinel-1 datasets might provide information, which leads to an understanding of the ASCAT trends and the general behaviour of microwave remote sensing data from urban areas.

1.2 Overview

The physical foundation and existing approaches to this problem are discussed in chapter two. In the third chapter the satellite systems and the derived products, which were used in the following chapter, are presented. The fourth chapter contains the creation of the different slopes and models and the processing steps leading up to them. The results of these datasets are presented in chapter five, which lead to the conclusions in chapter six.

2 State of the Art

2.1 Physical Foundation

SAR imaging systems transmit electromagnetic pulses which are reflected by the atmosphere and the earth's surface. The echoes are received back at the SAR system by a receiving antenna which can be the same as the transmit antenna or a separate system. There are different scattering mechanisms, which have to be modelled differently. Since present thesis focuses on the observation of urban areas, only non-volume scattering (which has to be considered when observing e.g., vegetation, ice and snow) and surfaces, where the penetration depth is not relevant, are discussed.

2.1.1 General Scattering Mechanisms

Roughness depends upon wavelength and incident angle (Figure 2-1). A surface is considered "rough" if its surface structure has dimensions comparable to the incident wavelength as stated by the Rayleigh criterion:

$$h > \frac{\lambda}{8 * \cos \theta}$$

(2-1)

h ... mean height of surface variations, λ ... wavelength, θ ... incidence angle
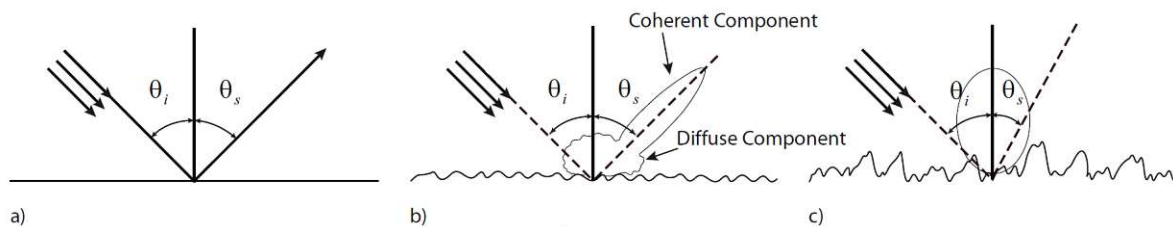

Figure 2-1. Scattering components for different surface roughness conditions: a) specular, b) slightly rough, c) very rough [1]

Urban areas are characterized by many smooth, highly reflective surfaces which are very different from naturally occurring surfaces. The combination of manmade materials such as glass, steel, concrete and tiles creates very distinctive backscatter patterns which stand out from surrounding vegetation.

2.1.2 Backscatter Mechanisms in Urban Areas

Three basic backscatter mechanisms that can be observed in urban areas are single, double and triple bounce scattering (see Figure 2-2).
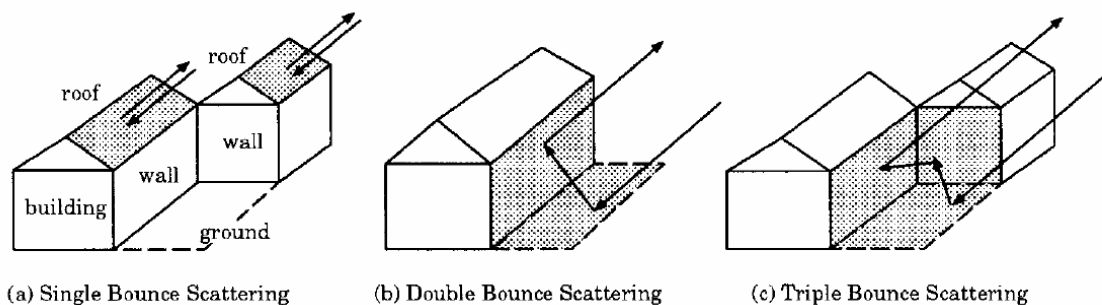

Figure 2-2. Backscatter mechanisms [2]

As stated by Y. Dong et al. [2, p. 1355] "the more bounces, the less backscattering response because the reflectivity of dielectric materials is less than 1." Single bounce scattering mostly comes from

tilted roofs. They are a strong specular reflector to the radar if the radar's incidence angle is close or the same to the tilt angle of the roof because the local incidence angle for the roof is in this case close to zero [2, p. 1355].
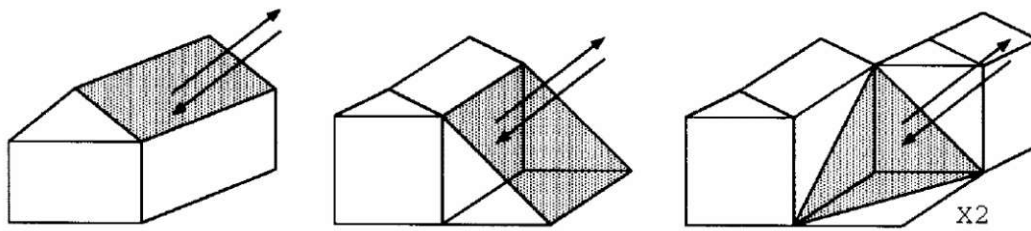

Figure 2-3. Projective areas illuminated by the radar for single, double and triple specular scattering mechanisms [2]

Double bounce behaviour like from a wall-ground structure results in a dihedral corner reflector as depicted in Figure 2-3. When comparing single to double bounce it is important to differentiate the polarization. For horizontal co-polarized (HH) radiation, one observes a 2 dB higher radar-cross-section (RCS) at single bounce than the RCS of the double bounce. For vertical co-polarized (VV) radiation the local incidence angle of the wall-ground structure is 60° which is close to the Brewster angle for the given dielectric constant. Therefore only a little of the incident field can be reflected by the wall surface, leading to a significant loss in the double bounce specular scattering. This leads to an about 18 dB lower RCS of the wall-ground structure than the RCS of the roof structure. These behaviours imply that the RCS of a wall-wall-ground structure (one more bounce) will be even lower even if the projected areas are the same as the ones from the wall-ground structure (Figure 2-3) [2, pp. 1355-1356].

The investigation of Y. Dong et al. [2] lead to the conclusion that the dominating factors of radar backscatter in urban areas are:

- Single bounce from roofs

- Double bounce from wall-ground structures

- Other metallic constituents

The other important factors highlighted in the paper are the incidence angle of the radar in regard to the tilt angle of the observed roofs and the polarisation response. If the satellite incidence angle and the roof angle are close to each other the single bounce dominates and the backscatter rises. Regarding the polarisation response a big contrast between urban areas and vegetation can be seen. In urban areas the co-polarized component is larger than that of the cross-polarized component. In contrast the cross-polarized component for forested areas is larger than the co-polarized component. For the present investigation the VV polarized datasets were used instead of the VH polarized ones because of the higher signal level and the higher sensitivity in urban areas.

2.1.3 Definition of "Urban Growth"

Due to the focus on areas, which are affected by urban growth, the term "Urban Growth" has to be specified. The definition of urban growth can be approached from many different perspectives. According to Clark [3], urban growth is a spatial and demographic process and refers to the increased importance of towns and cities as a concentration of population within a particular economy and society. It occurs when the population distribution changes from being largely hamlet and village based to being predominantly town and city dwelling.

In the book by Bhatta [4, p. 4] the most simplified definition of "urban growth" is "spatial growth of towns and cities". Because of the need of a concrete definition of urban growth for the creation of detection algorithms the definition "change from former grassland, woodland or agricultural areas to

at least manmade bare soil/paved areas" has been created. This definition is still quite broad, but the focus lies on effects, which can be detected by SAR systems and can be extracted by processing these datasets.

2.2 Existing Approaches

Most remote sensing based approaches of the detection of urban growth use datasets derived from multi-spectral sensor systems which typically use wavelengths in the visible and near-infrared spectrum. Datasets from different time periods are compared using various algorithms. As summarized by Bhatta [4, pp. 65-81] popular techniques are Image Overlay, Image Subtraction, Image Index, Spectral-Temporal Classification, Image Regression, Principal Components Analysis Transformation, Change Vector Analysis, Artificial Neural Network, Decision Tree, Intensity-Hue-Saturation Transformation, Econometric Panel, Image Classification and Post-classification Comparison. This list highlights the vast possibilities of processing steps that are available for the analysis of optical remote sensing data. The usage of sensor systems operating in visible/near infrared spectrum introduce following constraints which have no or nearly no impact on SAR based measurements:

- Atmospheric attenuation – different atmospheric condition and thereby different illumination in different image dates [4, p. 5]

- Changes in sun azimuth and elevation – difference in shadow effects and illumination [4, p. 5]

- Weather effects, especially clouds

There are also SAR-based approaches regarding the backscatter behaviour of urban areas. One example is the comparison of different radar sensors made by S. Frolkin et. al. [5], which showed that there is a strong linear correlation between ASCAT urban backscatter and a dataset of building volume of different urban areas on Europe, China and the USA.

2.3 Study Areas

The five chosen study areas contain the urban areas of Vienna, London, Abu Dhabi and Shanghai as well as the rural area around the small village Patzmannsdorf north of Vienna (see Figure 2-4). These areas have been selected because of their differences regarding urban growth, estimated backscatter behaviour and satellite coverage (see Table 2-1).
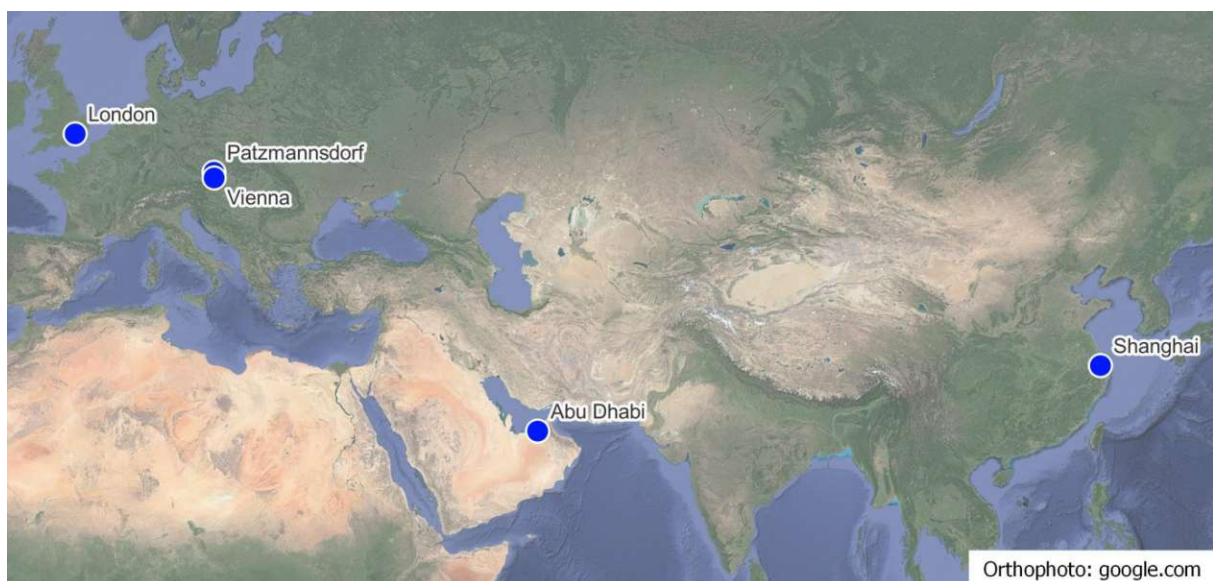

Orthophoto: google.com

Figure 2-4. Location of the five study areas

2.3.1   Vienna

The city of Vienna covers an area of over 400 km² which is zoned in ~15 km² of built-up land, ~19 km² grassland, ~2 km² water bodies and ~6 km² traffic areas [6] and inhabits over 1.9 million people [7]. This shows a quite even spread between densely populated and rural areas, which continue around the city itself. The urban share decreases along with the distance to the city centre, especially to the north and west of Vienna. This region has been chosen because of the author's knowledge about the city development. Between the years of 2015 and 2019 the population rose by 5.6 percent [8]. Comparison of land cover data sets showed that from 2015 to 2019 the area saw an increase in urban areas by 0.24 percent.

2.3.2   London

The capital of the United Kingdom spreads over 1.572 km² and inhabits almost 9 million people. Between 2015 and 2019 the population rose by over 4 percent [8]. The area of interest consists almost completely of built-up areas. Its backscatter behaviour and satellite coverage should be similar to the Viennese region which should help in determining the stability of the data acquisition. Comparison of land cover data sets showed that from 2015 to 2019 the area saw a slight increase in urban areas by 0.06 percent.

2.3.3   Abu Dhabi

The city of Abu Dhabi spreads over an area of 972 km² and inhabits a population of 1.5 million. The population rises fast with an increase of over 20 percent between the years 2015 and 2019 [9]. The area has been chosen because of its position in the desert and therefore the contrast between urban areas and barren land. Comparison of land cover datasets showed that from 2015 to 2019 the area saw an increase in urban areas by 0.15 percent.

2.3.4   Shanghai

Shanghai inhabits over 28 million people and covers an area of 6.340 km². Between the years of 2015 and 2019 the population count increased by over 12 percent [9]. This city is the biggest urban area investigated in this thesis where almost the entire city has been covered with urban structures. Comparison of land cover data sets showed that from 2015 to 2019 the area saw a significant increase in urban areas by 4.2 percent.

2.3.5   Patzmannsdorf

The area surrounding the village Patzmannsdorf is almost completely covered by cropland with just a few other villages and industrial complexes scattered in between. The small village had a decline of over 4 percent in population between 2015 and 2018 [10]. Comparison of land cover data sets showed that from 2015 to 2019 the area saw almost no increase (0.01 percent) of urban areas. This rural area has been chosen as a comparison area for a better isolation of urban – only backscatter behaviour.

Table 2-1. Summary of important metrics of the study areas

	Vienna	Patzmannsdorf area	London	Abu Dhabi	Shanghai
Population (Mio)	1.9	0	9	1.5	28
Population growth 2015-2019	5.6%	-4%	4%	20%	12%
Urban area increase	0.24%	0.01%	0.06%	0.15%	4.2%

2.4 Sensor Systems

In this thesis datasets containing data collected by two different sensor systems from two separate satellite missions are used.

2.4.1 ASCAT

The Advanced Scatterometer (ASCAT) located on the MetOp meteorological satellites is an active microwave remote sensing instrument initially designed for monitoring winds over the oceans. However, numerous experiments showed that ASCAT is more versatile than initially assumed. It operates at a vertically polarized C-band frequency with a nominal resolution of 50km or 25km for the high resolution variant [11].

2.4.2 Sentinel-1 C-SAR

The satellites of the Sentinel-1 mission feature an active phased array antenna called the C-SAR instrument. As the ASCAT it operates at a C-band frequency but at different polarisations. Also its resolution is much higher with up to 5x5 m resolution depending on the chosen acquisition mode [12]. The Sentinel-1 mission is designed to cover different, large and small scale, implementations and products e.g. oil spill detection, sea ice monitoring, emergency services, mapping of land and analyzing vegetation coverage [13]. To cover such diverse use cases the Sentinel-1 SAR instrument supports four different imaging modes which provide different resolution and coverage (Table 2-2).

Table 2-2. Sentinel-1 swath modes [12]

Mode	Incidence Angle	Resolution	Swath Width	Polarization (H = Horizontal; V = Vertical)
Stripmap	20 - 45	5 x 5 m	80 km	HH+HV, VH+VV, HH, VV
Interferometric Wide swath	29 - 46	5 x 20 m	250 km	HH+HV, VH+VV, HH, VV
Extra Wide swath	19 - 47	20 x 40 m	400 km	HH+HV, VH+VV, HH, VV
Wave	22 - 35 35 - 38	5 x 5 m	20 x 20 km	HH, VV

3   Datasets and Region of Interests

3.1   Study Sites

As mentioned in chapter 2.3 the five study areas feature unique backscatter behaviours which result in different ASCAT and Sentinel-1 backscatter trend curves. For an approximated delineation of the hamming window a circle with a diameter of 30km was first chosen for the boundary of the areas of interest, which is further described in chapter 4.2.2. The following overview in Figure 3-1 and the description of the land cover has been created using the land cover data from the Copernicus Global Land Operations Global 2015 dataset with 100m resolution [14].

3.1.1   Vienna

The area enclosed by the 30km radius circle contains a mixture of urban, rural and forest areas. The areas north of Vienna, where most urban growth happened during the last years, are not enclosed and therefore not included in the results.

3.1.2   Patzmannsdorf

The area of interest contains mostly cropland with a large forest in the south and a smaller one in the northwest of the 30km radius. There are many small villages scattered across the area of interest with a larger one in the northwest.

3.1.3   London

As second urban European region the city of London and its surroundings have been chosen. The middle of the circle is roughly 5 kilometres north from the city centre. The circle itself contains mostly built-up areas with some vegetated areas (mostly parks) and water bodies. A few croplands are located at the outer border of the circle.
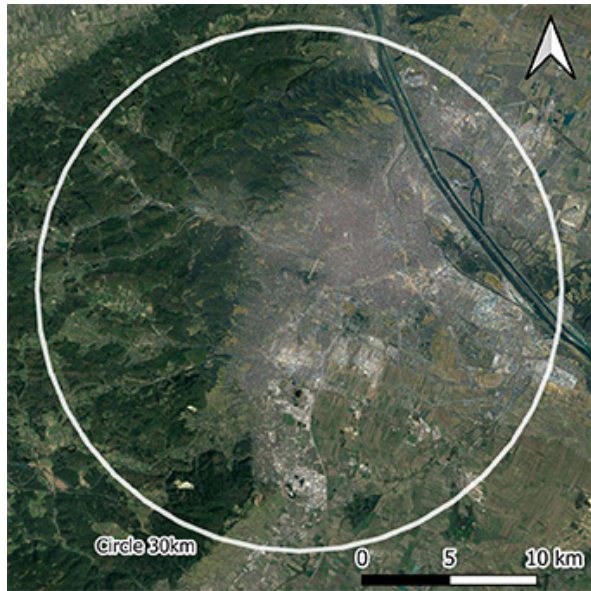
3.1.4   Abu Dhabi

The city at the Persian Gulf is located in an area of mainly deserted and bare soil with few vegetated areas which are mostly manmade. The middle of the Abu Dhabi circle lies approximately 24 kilometres southeast from the city centre and contains smaller urban areas. Aside from smaller manmade parks in the southwest and the built up areas the region consists almost completely of bare soil /sparse vegetation.
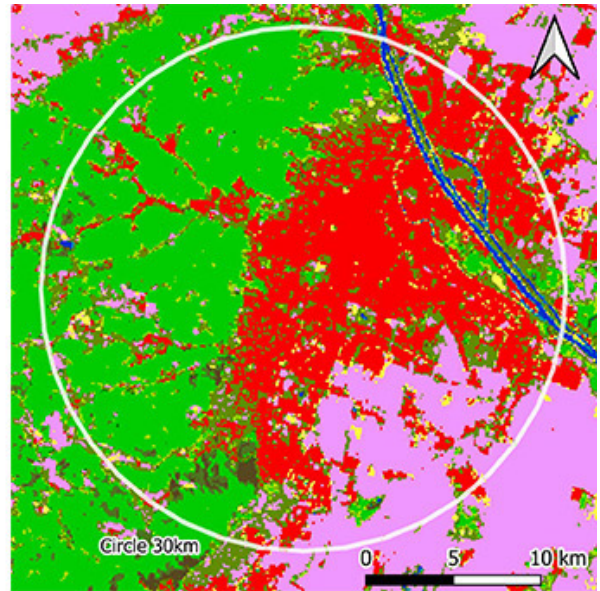
3.1.5   Shanghai

In the dataset of Shanghai the area of interest is almost centred at the city centre and, besides small cropland areas and the river, the radius covers urban regions.
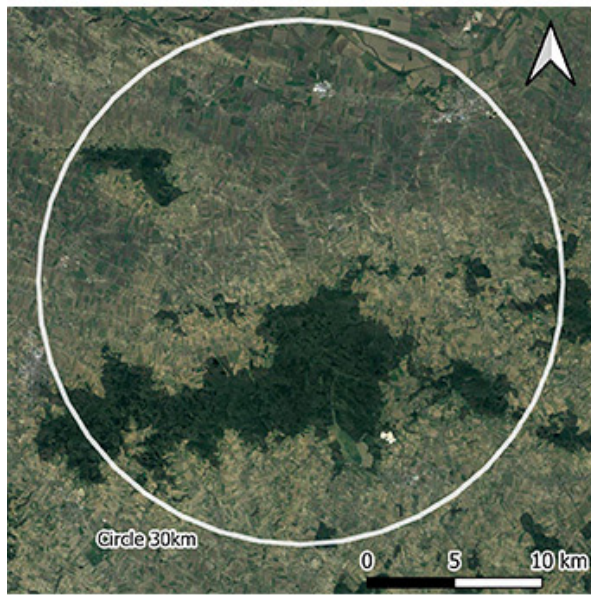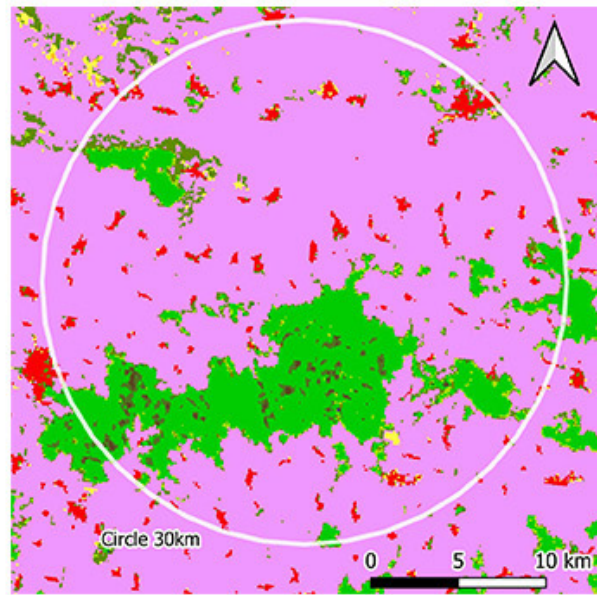
a)

b)

c)

d)

e)

f)

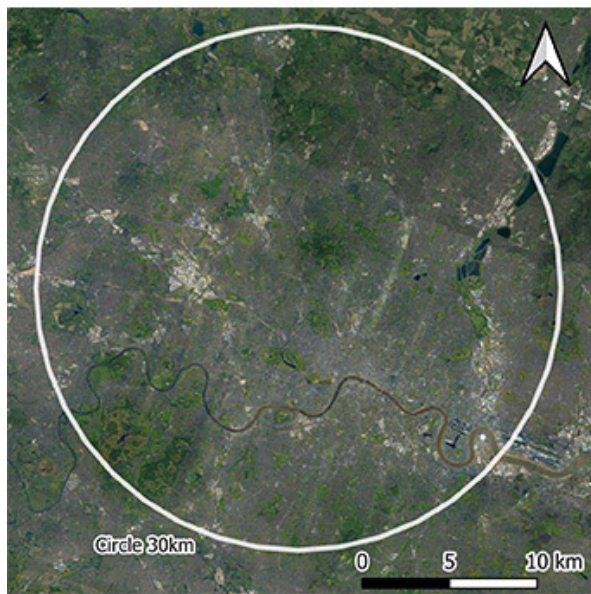|			
■ No input data available	■ Permanent Water Bodies	■ Deciduous broadleaf closed forest	■ Deciduous broadleaf open forest
■ Shrubland	■ Herbaceous Wetland	■ Mixed closed forest type	■ Mixed open forest type
■ Herbaceous vegetation	■ Moss & lichen	■ Unknown closed forest type	■ Unknown open forest type
■ Cropland	■ Evergreen needleleaf closed forest	■ Evergreen needleleaf open forest	■ Ocean
■ Built-up	■ Evergreen broadleaf closed forest	■ Evergreen broadleaf open forest	
■ Bare / sparse vegetation	■ Deciduous needleleaf closed forest	■ Deciduous needleleaf open forest	

Figure 3-1. Satellite images (Landsat/Copernicus extracted from Google Earth) and land cover [14] datasets of the areas of interest with the chosen 30km radius. a),b) Vienna. c),d) Patzmannsdorf. e),f) London. g),h) Abu Dhabi. i),j) Shanghai.

14

3.2 ASCAT Dataset

Since the measured grid has an orbit-aligned geometry the data is resampled to a discrete global grid (DGG) with global equidistant sampling of 12.5 km. A 34 km search radius around each DGG Point is used for collocation, the weighting is realized using the so called 'Hamming Window Function'. More weight is assigned to the points closer to the centre value with declining weight the further away the measurements are from the centre. Using this weighting function datapoints were calculated and put together in a backscatter time series [15].

3.2.1 ASCAT Backscatter Model Time Series

The provided ASCAT dataset features a daily backscatter signal from January 2007 until December 2020. The European region datasets consist of roughly double the data points than the Asian and African datasets (see Table 3-1). The comparably low number of measurements of the Abu Dhabi region is caused by the combination of the polar satellite orbit and its location close to the equator. Additionally to this effect the Shanghai region is also affected by its close proximity to the sea because measurements containing a large amount of open water were excluded during resampling.

Table 3-1. ASCAT measurement details

	Vienna	Patzmannsdorf	London	Abu Dhabi	Shanghai
Data points	9832	9229	10818	6342	5397
Signal mean	-6.39 dB	-9.76 dB	-4.33 dB	-13.40 dB	-2.54 dB
Mean signal increase (2007-2021)	0.80 dB	0.22 dB	0.86 dB	3.15 dB	2.47 dB

Especially in urban environments a significant increase in backscatter signal can be observed in the given time frame. In the rural area dataset of the Patzmannsdorf region there is no significant increase in backscatter to be observed, just the variations in backscatter caused by the vegetation and other season-based influences. The trend in the other datasets could be explained by the growth of urban areas in these regions.

3.2.2 Regional Characteristics of ASCAT Datasets

3.2.2.1 *Vienna*

In the urban dataset of Vienna an average increase of ~0.06 dB per year can be observed (see Figure 3-2). The areas north of Vienna, where most urban growth happened during the last years, is not covered by the ASCAT pixel, which could explain the steady increase in backscatter instead of a sudden one. Due to the significant amount of vegetation inside the ASCAT pixel there are seasonal variations visible in the data.
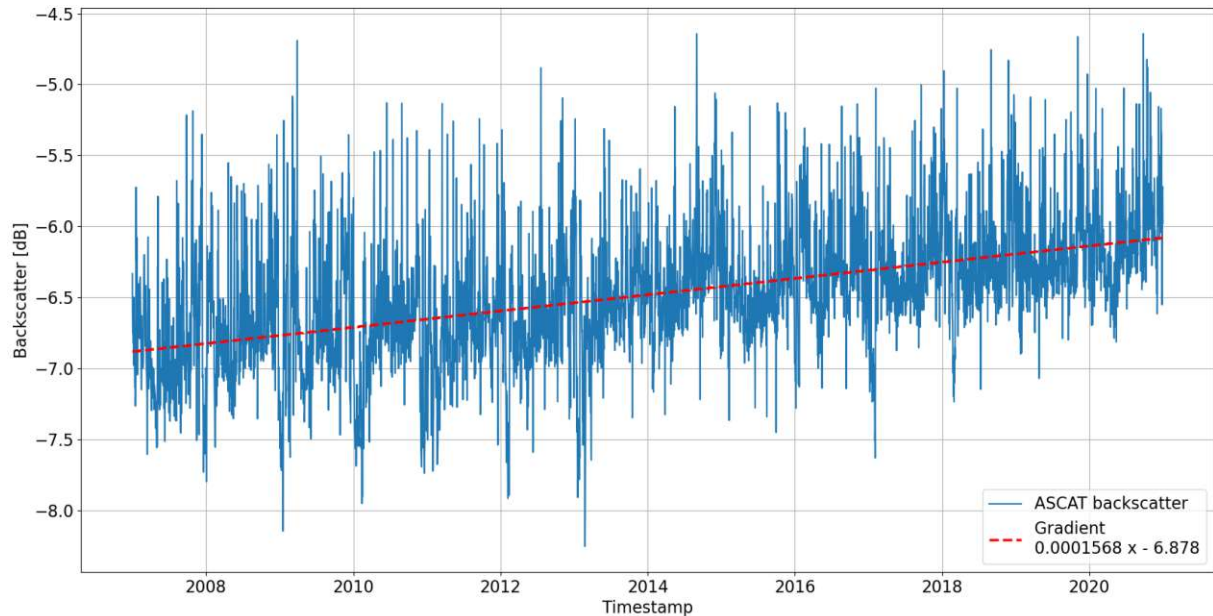

Figure 3-2. ASCAT backscatter time series Vienna

3.2.2.2 *Patzmannsdorf*

As a reference dataset for rural data the region around the village Patzmannsdorf in Austria has been chosen. Because of the high amount of vegetation and agriculture there is a much higher amount of seasonal variation in the data than in the other datasets. In contrast, there is a very small positive trend of just ~0.016 dB per year present (see Figure 3-3). Apart from the seasonal variations no significant trend can be observed in the data.
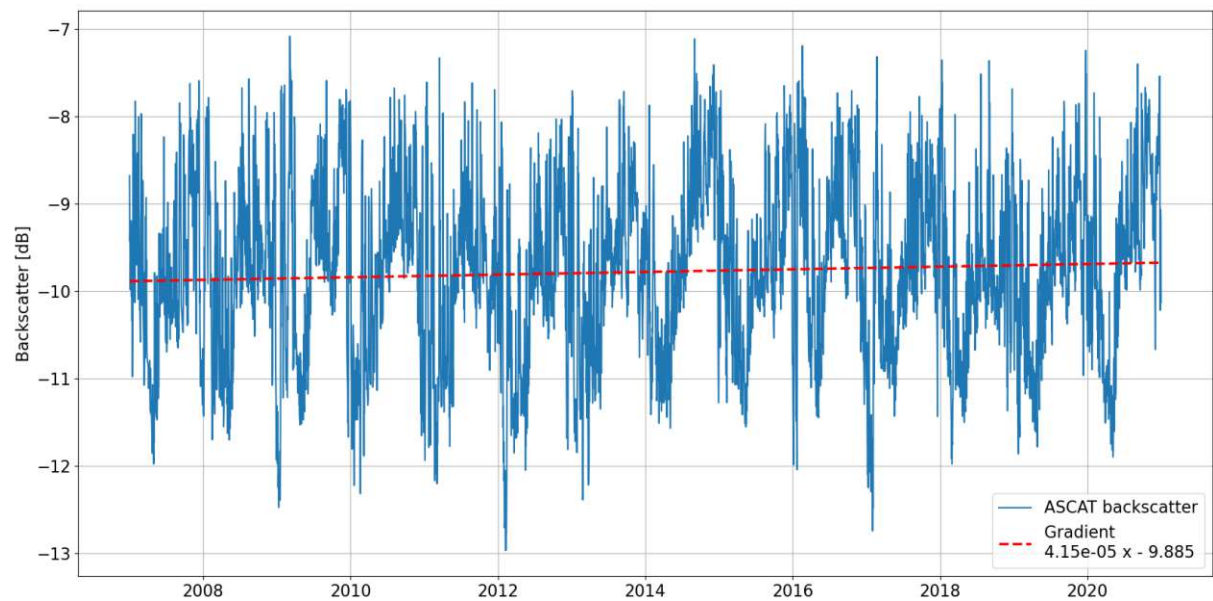
Figure 3-3. ASCAT backscatter time series Patzmannsdorf

3.2.2.3 London

The mean yearly increase of the backscatter data is ~0.05 dB, which is comparable to the Vienna dataset despite the fact that the overall region is much more built-up than the region of Vienna (see Figure 3-4). There are also forested areas present, which could explain the significant seasonal variation in the backscatter data. Moreover, the overall signal level is much higher than in the previous datasets.
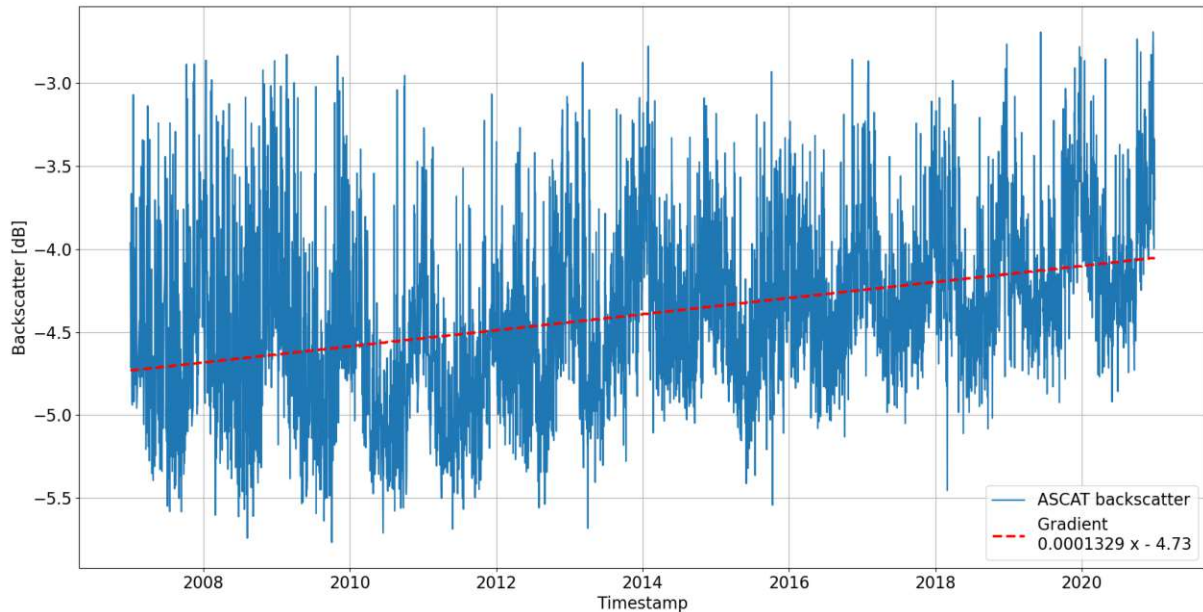

Figure 3-4. ASCAT backscatter time series London

3.2.2.4 Abu Dhabi

The almost complete absence of vegetation explains the very small seasonal variations in the Abu Dhabi dataset. The mean increase of the ASCAT backscatter trend is around 0.23 dB per year, which is higher than that of the European regions (see Figure 3-5). From 2017 onwards the increase in backscatter is lowering and the trend seems to flatten compared to the previous years.
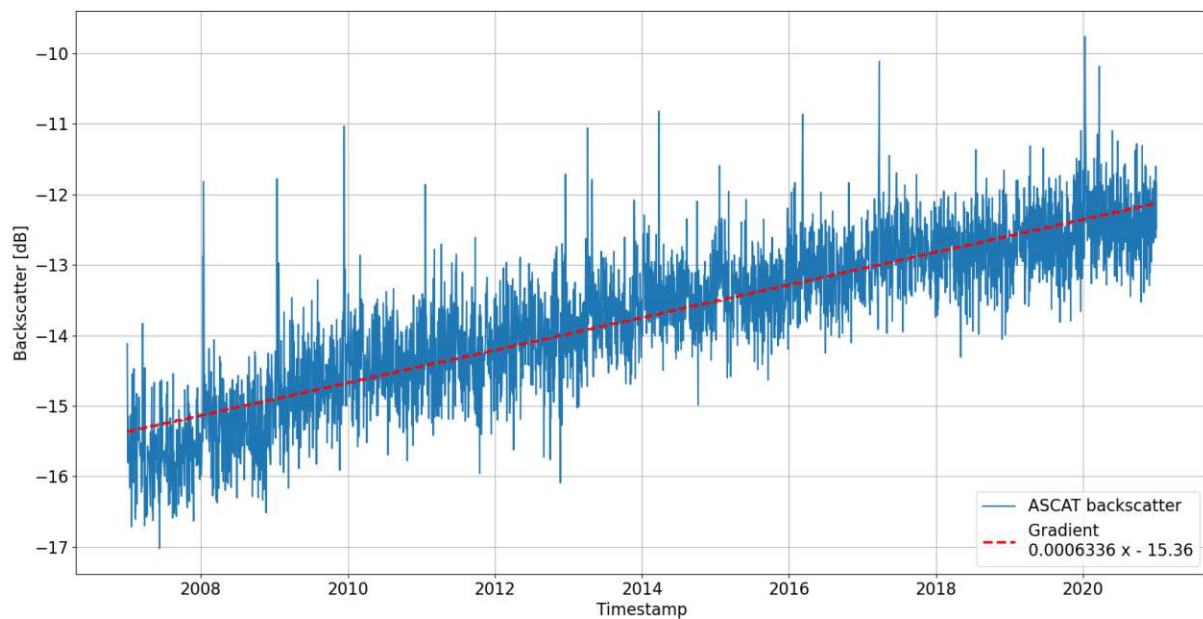
Figure 3-5. ASCAT backscatter time series Abu Dhabi

3.2.2.5 Shanghai

The observed mean in the yearly increase of the Shanghai dataset is about 0.17 dB, which is comparable to the one from the Abu Dhabi dataset (see Figure 3-7). From the beginning of 2016 onwards the trend curve flattens and there seems to be almost no further increase of the mean signal level. This could mean that the expansion of urban areas has reached the outer edges of the investigated area and now there are nearly no areas left, which could be converted from rural into built up regions.
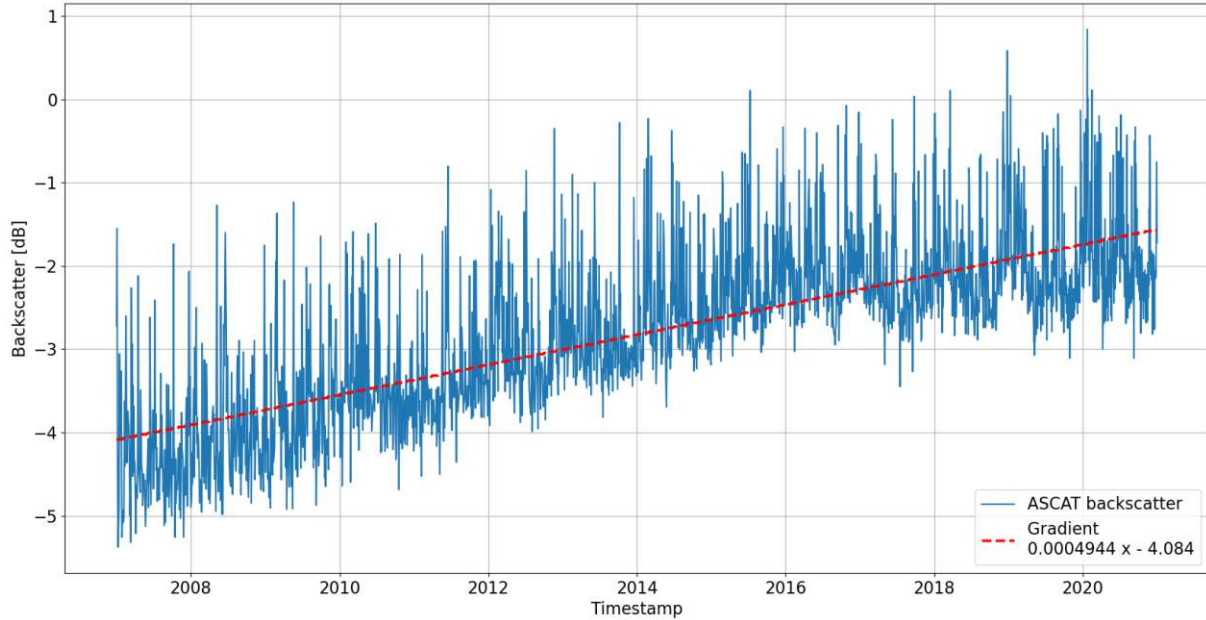

Figure 3-6. ASCAT backscatter time series Shanghai

3.3 Sentinel-1 Monthly Means 2016-2019

3.3.1 Sentinel-1 Mission

As part of the Copernicus space component, the Sentinel-1 (S1) mission is implemented through a constellation of two satellites (A and B units) each carrying an imaging C-band SAR instrument providing data continuity of the ERS and ENVISAT SAR missions (see Figure 3-7). Each Sentinel-1 satellite is designed for an operational lifetime of 7 years with consumables for 12 years. The Sentinel-1 satellites fly in a near polar, sun-synchronized (dawn-dusk) orbit at 693 km altitude. Each of the satellites has a 12 day repeat cycle with 175 orbits per cycle. The usage of two satellites lowers the revisit time to six days [12].
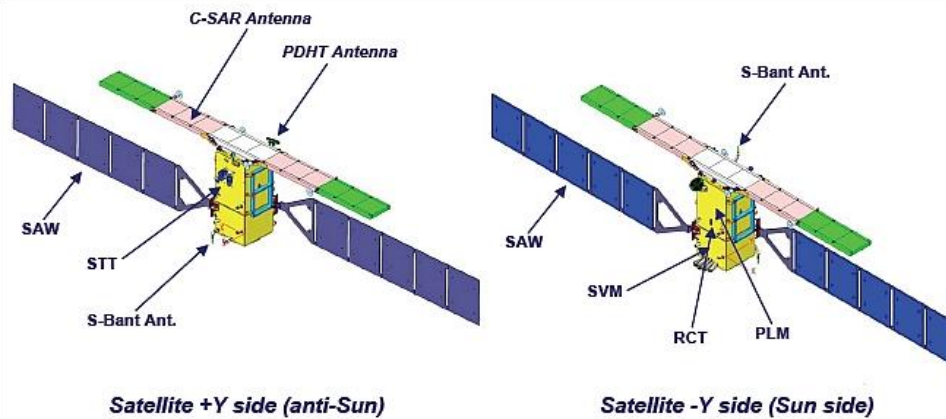
Figure 3-7. Sentinel satellite composition [12]

3.3.2 Sentinel-1 Data Processing

The provided Sentinel-1 dataset consists of 100km x 100km size monthly means from January 2015 until December 2018 in 10m x 10m pixel resolution in VV and VH polarisations. They were created by processing Sentinel-1 data by the TUWGEO for the Austrian Data Cube (ACube) service. Ground Range Detected (GRD), Interferometric Wide (IW) swath, and high-resolution (H) Synthetic Aperture Radar (SAR) data (Level-1) from Sentinel-1's C-band sensors serve as input to ACubes' processing engine. A high-resolution digital terrain model (DTM) at 10m sampling was utilised to guarantee the best possible geocoding accuracy. This DTM was derived from Airborne Laser Scanning (ALS) data.

The main workflow responsible for pre-processing, using the SAR Geophysical Retrieval Toolbox A01 workflow, consists of the following steps [16]:

- Applying external, precise orbit data

- Removing border noise pixels, which are present at an early stage of the mission. They were introduced by the transition from Level-0 to Level-1, conducted by the Instrument Processing Facility (IPF). In March 2018, IPF released a new processor version (IPF 2.90), which does not produce such artefacts at the image borders anymore.

- Low backscatter from flat surfaces (e.g. lakes, rivers or streets) is close to the signal-to-noise ratio (SNR) of the sensor increasing the amount of measured noise, also known as thermal noise. Its contribution to the observed signal is reduced in this step by applying the thermal noise calibration vectors stored in the Level-1 metadata.

- Performing radiometric calibration to get sigma nought based on a unit area on the ellipsoid.

- Resampling calibrated backscatter values from orbit to ground geometry using Range-Doppler terrain correction with the prepared external DEM in ellipsoid heights.

- Applying some postprocessing, e.g., conversion to dB units.

- Regridding and tiling the scene given in the geographic CRS to the Equi7Grid system.

The following steps were performed to create monthly averaged backscatter images with SGRT's B01 workflow.

The separation of orbits can be ignored since the average backscatter per month is of main interest.

- Collecting all files for each month, each polarisation and each tile within the time span and tile set of interest.

- Loading the monthly datacube iteratively into memory and decode it to dB values and set NaN values.

- Converting dB values into linear units.

- Averaging over all values along the temporal dimension, ignoring NaN values.

- Converting linear to dB units.

- Iteratively writing reduced data to disk.

The amount of Sentinel-1 passes and therefore the numbers of measurements, which have been aggregated for the monthly means, vary greatly depending on the region of interest as can be seen in Figure 3-8. The first large difference between the datasets is the difference between the European and the other datasets. The second distinctive feature is the rise in measurements from mid 2016 to the beginning of 2017.
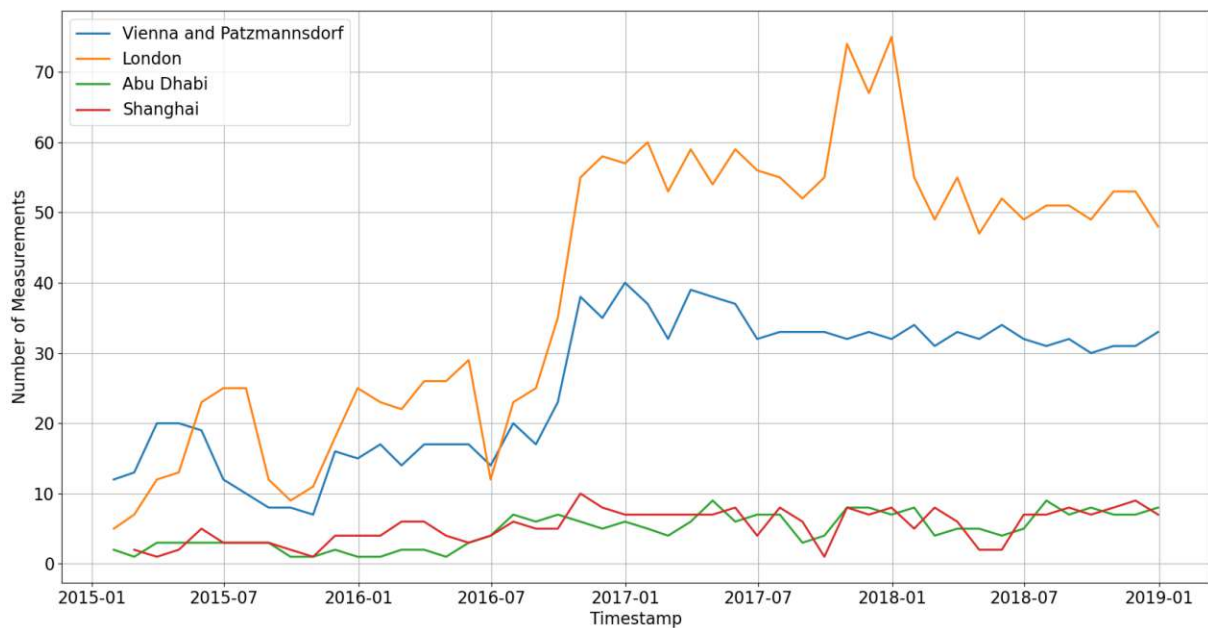
Figure 3-8. Number of monthly Sentinel-1 measurements

3.3.3 Dataset Errors

In the Abu Dhabi dataset interference patterns, which were probably caused by radio interference, are present. They lead to significant errors in the calculated gradient map (see Figure 3-9). The affected data tile had to be removed to avoid errors during the gradient map calculation.

Figure 3-9. Presumable RFI effects affecting a Sentinel-1 data tile of the Abu Dhabi region

4 Methodology

The datasets derived from the two sensor systems differ greatly in regards of temporal and spatial resolution. Therefore the investigation of the correlation between the two datasets is the first step. The idea behind this approach is, that in case of a high correlation, the analysis of the Sentinel-1 datasets could lead to the conclusion, which small-scale backscatter mechanisms influence the ASCAT backscatter and lead to the trends in both datasets.

4.1 Working Environment

The following processing steps were done using Python 3.6. The raster image visualisation and the creation of shapefile masks were generated with the open-source geoinformation system QGIS. The results have been compared with optical data extracted from Google Earth because of the integrated timelapse feature.

4.2 Data Preparation

Before the calculation of correlation factors, the two datasets have to be resampled to the same temporal and spatial scale. To match the ASCAT hamming window, circles with diameters of 20km and 30km centred at the ASCAT midpoint of each region were created. The Sentinel-1 tiles were cut to the size of these circles. This was done using shape masks, which were converted into OGR polygons and rasterized resulting in array masks with which the tiles were masked. After masking the images, the mean of all remaining pixel values has been calculated. This was done for each month which resulted in a list of 48 mean values which represent the Sentinel-1 trend. The ASCAT values have been aggregated monthly to achieve the same temporal sampling as the Sentinel-1 trend (see Figure 4-1).

Define target area	• Create shapefile mask • Convert shapefile to OGR polygon mask
Clip dataset	• Mask the Sentinel-1 datasets of each month to fit ASCAT extent
Stitching	• If more than one tile is affected: Stitch datasets together
Mean calculation	• Calculate the mean of the backscatter pixel values for each time stamp
ASCAT import	• Load ASCAT data and resample to monthly values
Calculate gradients	• Calculate linear gradients for the S1 and the ASCAT trend curves and the statistical parameters
Plot creation	• Create trend curve plots including all relevant metrics and statistical parameters

Figure 4-1. Main processing steps

4.2.1 Temporal Fit

After processing both datasets and the creation of the trends, the two resulting graphs were compared. In all regions there were significant differences between both curves between January 2015 and circa January 2017. These variations stop with the commissioning of Sentinel-1B and the Sentinel-1 data became much more stable. Because of the inconsistency before the introduction of Sentinel-1B the timeframe of the Sentinel-1 data has been reduced to the datasets from January 2017 to the end of 2019. In the Abu Dhabi dataset, an outlier at timestamp 08/2017 is present. This is caused by insufficient satellite passes of the specific area during this month which resulted in an almost empty tile. For the comparison of the ASCAT and Sentinel-1 slopes this outlier has been removed and its mean has been interpolated between the two neighbouring mean points.

4.2.2 Spatial Fit

After analysing all five areas of interest using circles of 20 km and 30 km diameter, very little differences between the overall behaviour of the datasets can be observed. Comparing just the mean trend gradients of the Vienna region, the 20 km circle shows almost no deviation where the 30 km circle deviates slightly. Contrary the behaviour of the Sentinel-1 trend from July of 2018 until the end of the dataset resembles the trend of the ASCAT trend curve more closely. Because of this small impact on the resulting trend behaviour a uniform circle size of 30 km diameter has been chosen to achieve bigger areas of interest and therefore more possibilities of in-depth analysis.

4.3 Mean Calculation

After the temporal and spatial fit of the Sentinel-1 datasets the pixel values of each timestamp were converted from logarithmic into linear values. For each timestamp the mean value of the linear pixel values was calculated. Prior to the trend curve plot the resulting mean arrays were converted back into the logarithmic space.

4.3.1 Trend Correlation

The Sentinel-1 and ASCAT trend curves were correlated with the Pearson correlation coefficient using the *corrcoef* function of the *numpy* library.

4.4 Gradient Map Creation

For the detection of temporal changes in the Sentinel-1 datasets pixel gradients were calculated. The time period of the Sentinel-1 input data has also been reduced to the January 2017 – December 2018 time period because of the much more consistent data. The resulting maps provide a baseline for a detailed investigation of different backscatter effects. The hypothetical reasons for positive and negative gradient values are:

Positive Gradients:

- New buildings/structures on former bare soil

- Expansion or modification of existing buildings/structures with more reflective materials and/or modifications which results in a more reflective geometry

- Changes in seed of cropland and change of the field direction

Negative Gradients:

- Removal of reflective buildings/structures/objects

- Changes in seed of cropland and change of the field direction

For each 10x10m position of the investigated area a gradient between the 48 pixels (one for each month) is calculated using the gradient of the linear regression function.

$$g = \frac{n(\sum xy) - (\sum x) * (\sum y)}{n(\sum x^2) - (\sum x)^2}$$
(4-1)

The function returns the gradient value for each pixel allowing the analysis of spatial patterns of temporal trends (see the results in chapter 5.2). The resulting gradient maps are used to locate regions with significant changes in the backscatter behaviour in the given timeframe. Especially urban area growth is a dominant source of positive gradient values. From the gradient maps the statistical distribution of pixel values are calculated to gain a better understanding of the behaviour of the different regions.
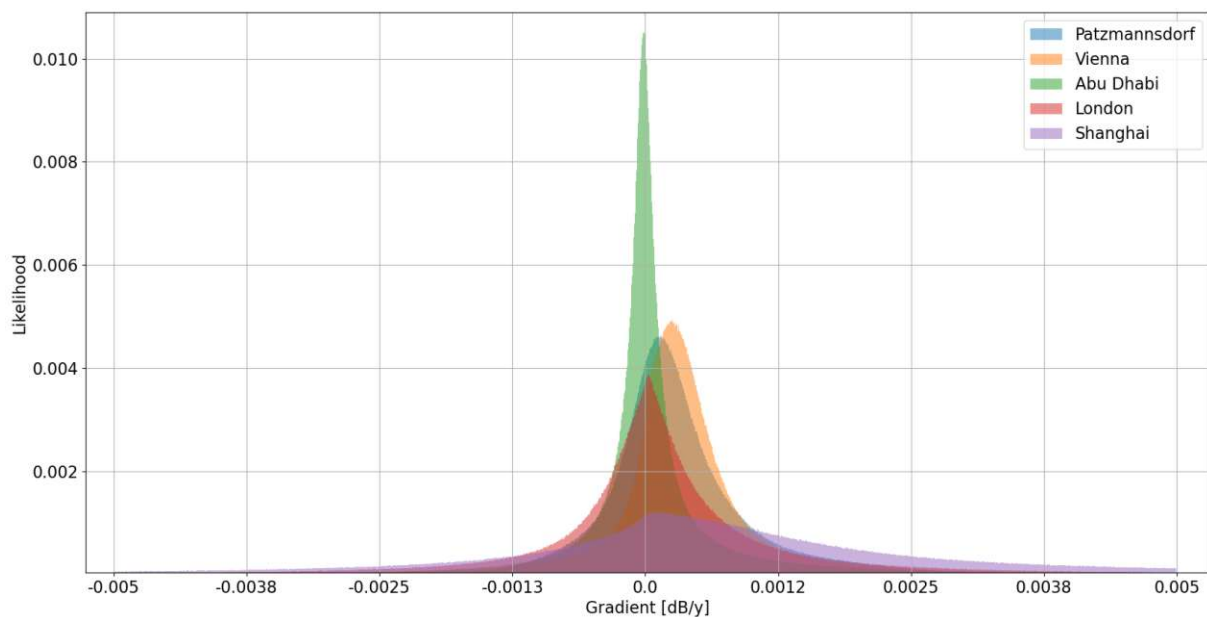
Figure 4-2. Gradient histogram comparison of the different regions
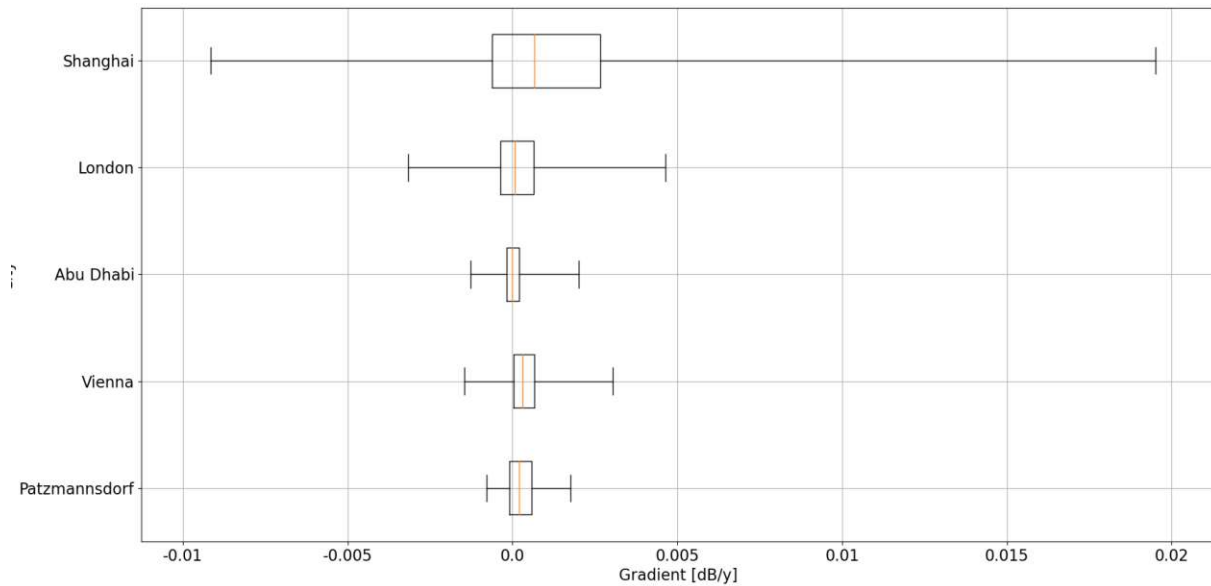
Figure 4-3. Gradient box plot comparison of the different regions

The comparison of the data distribution of the gradient maps shows distinctive differences between the datasets. While the European datasets show a quite comparable spread, with small differences in mean values, the other two regions differ vastly (Figure 4-2). The region of Abu Dhabi has a much smaller spread of pixel values, which is caused by the large amount of desert area in the observed area, which produces very low backscatter values. In contrast the Shanghai dataset shows a very widespread plot of pixel values which is caused by the large share of urban area in the pixel region. Except the Abu Dhabi region (which has a gradient of almost zero) all datasets share a positive gradient.

4.5 Classification and Masking of Urban Areas

To extract urban areas for further analysis and better understanding of the backscatter behaviour in areas with urban change the approach of masking based on backscatter values has been chosen. This was done by choosing specific backscatter thresholds which were found through iterative testing.

Following the findings of preceding tests the chosen thresholds are applied:
If VH > -13 dB AND VV > -6 dB: TRUE – otherwise: FALSE

The combination of VV and VH thresholds was used to eliminate misclassifications in rural areas. This classification has been done for each timestamp of the 2017-2019 time period which resulted in 48 monthly classification pictures per region. Using different logical functions the following three masks have been created:

- **Maximum Extent**

  Using the logical OR function all pixels which were classified as urban at least once are shown as TRUE

- **Minimum Extent**

  Using the logical AND function all pixels which were classified as urban in each of the 48 pictures are shown as TRUE

- **Single Urban Growth**

  A function was created which compares each of the 48 pictures if there has been a single consistent flip from non-urban to urban which remains throughout the whole dataset

5 Results and Discussion

After the preliminary steps of fitting the datasets temporally and spatially, as discussed in chapters 4.2.1 and 4.2.2, the different algorithms have been carried out starting with the calculation and comparison of the trend curves.

5.1 Trend Comparison

The first step of analysis was the correlation of the ASCAT and Sentinel-1 trends. The reason behind this step was the assumption that further in-depth analysis can be done reliably if the Sentinel-1 dataset provides a similar behaviour as the ASCAT dataset.

5.1.1 Vienna

Comparing the complete ASCAT timeline with the 2017 – 2019 trend from Sentinel-1 the first obvious difference is the much steeper gradient incline of the Sentinel-1 trend (see Figure 5-1). This is caused by the local incline in backscatter signal between 2017 and 2019, which is much higher than the mean incline of the complete ASCAT trend (see Figure 5-2).
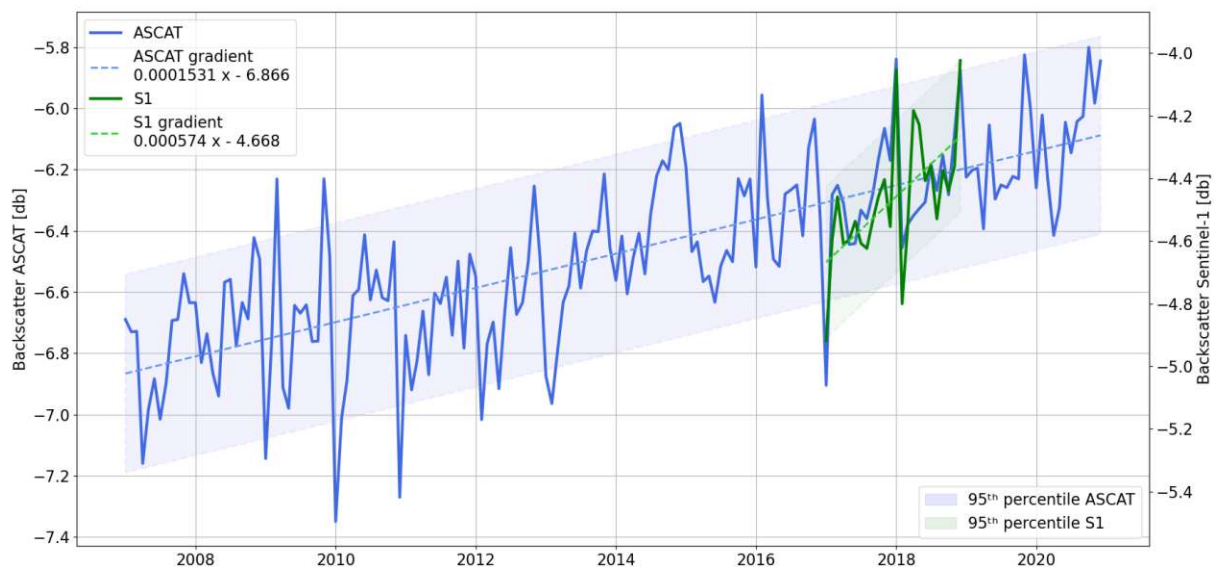
Figure 5-1. Comparison of the complete ASCAT trend with the 2017 – 2019 Sentinel-1 trend of Vienna

Comparing the two trend curves at the same time extent they and their respective gradients line up very well, which makes further in-depth analysis possible for the Vienna dataset.
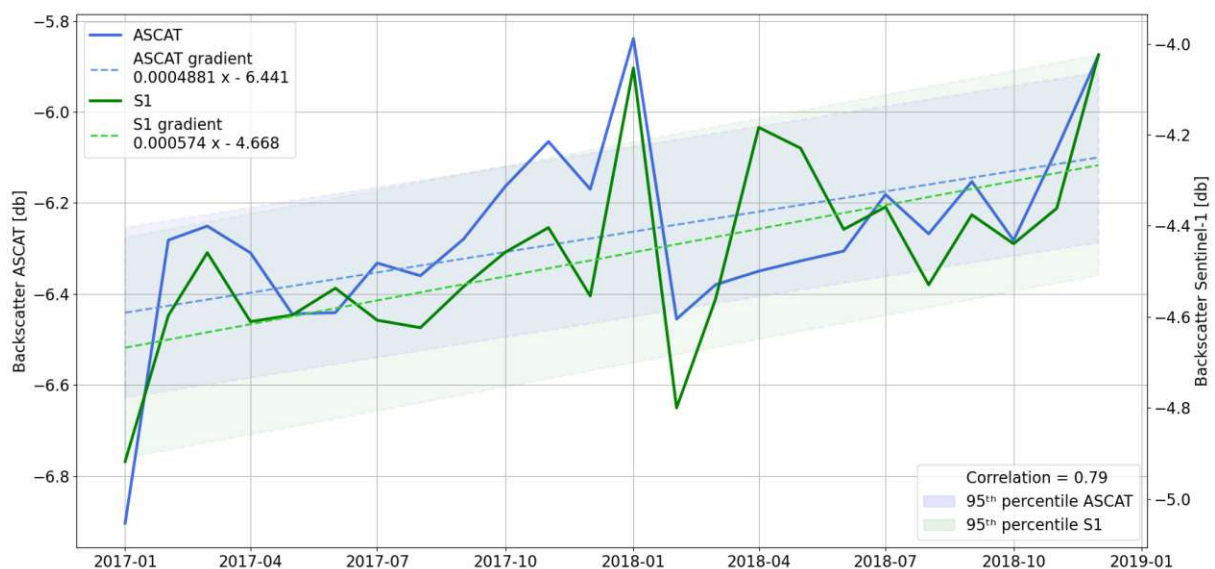
Figure 5-2. Comparison 2017 – 2019 Sentinel-1 – ASCAT monthly mean trend curves of Vienna

5.1.2   Patzmannsdorf

The 2017 – 2019 Sentinel-1 values from the Patzmannsdorf dataset have an even steeper gradient incline compared to the quite flat gradient of the complete ASCAT trend (see Figure 5-3).
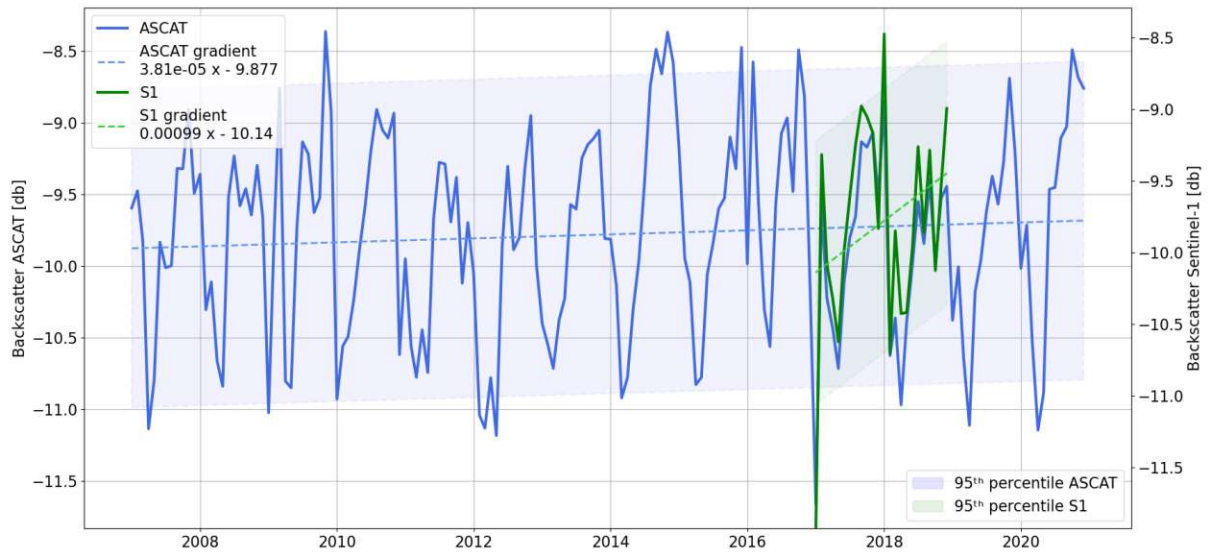
Figure 5-3. Comparison of the complete ASCAT trend with the 2017 – 2019 Sentinel-1 trend of Patzmannsdorf

After reducing the Sentinel-1 extent to the two-year period the two trends correspond well, which renders the Patzmannsdorf region suitable for further experiments. Even small details present in each trend curve match really well and lead to a correlation factor of 0.95 (see Figure 5-4).
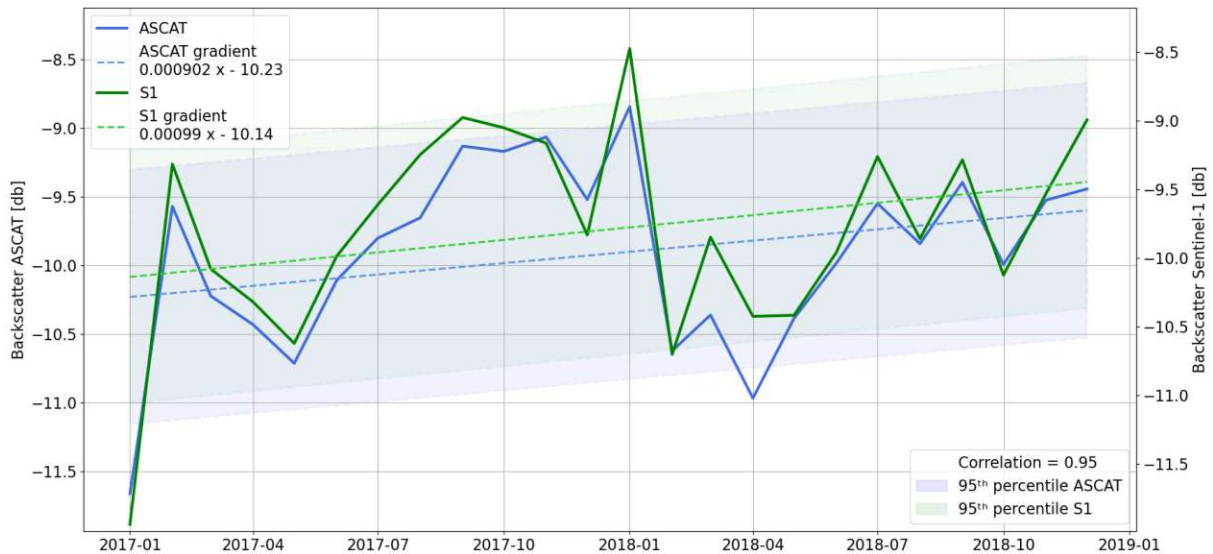
Figure 5-4. Comparison 2017 – 2019 Sentinel-1 – ASCAT monthly mean trend curves of Patzmannsdorf

5.1.3 London

Similarly to the previously analyzed datasets the two trend curves from the London dataset correlate very well even when comparing the Sentinel-1 two-year trend with the complete ASCAT trend (see Figure 5-5).
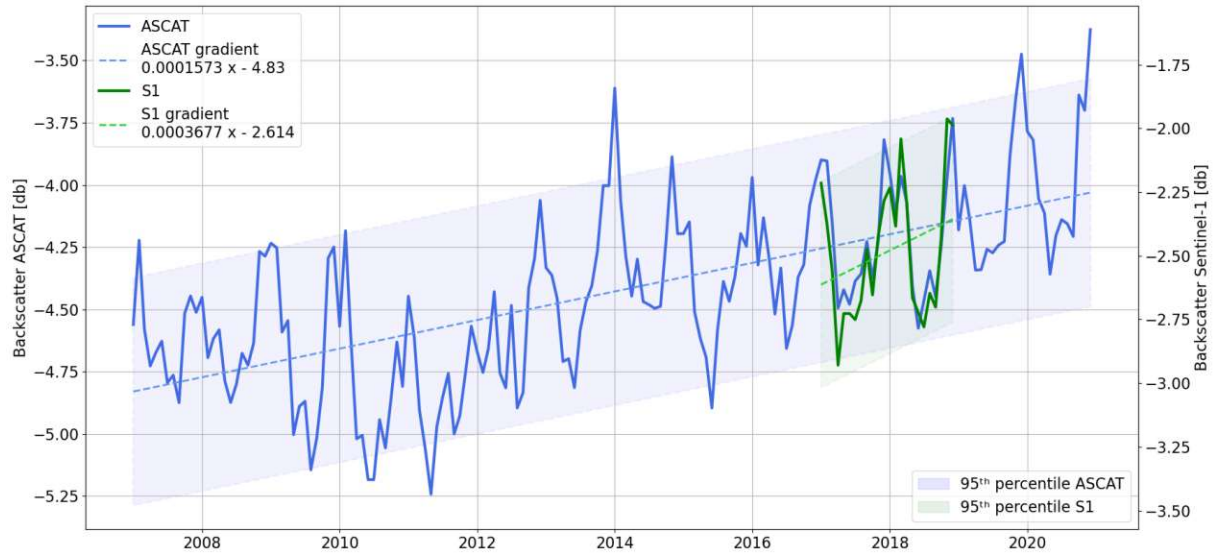
Figure 5-5. Comparison of the complete ASCAT trend with the 2017 – 2019 Sentinel-1 trend curves of London

The comparison of the two-year trends shows that the Sentinel-1 dataset has a steeper gradient slope than the ASCAT dataset but overall the behavior of the two trend curves shows a high correlation (see Figure 5-6). This makes this region of interest also suitable for more detailed analysis.
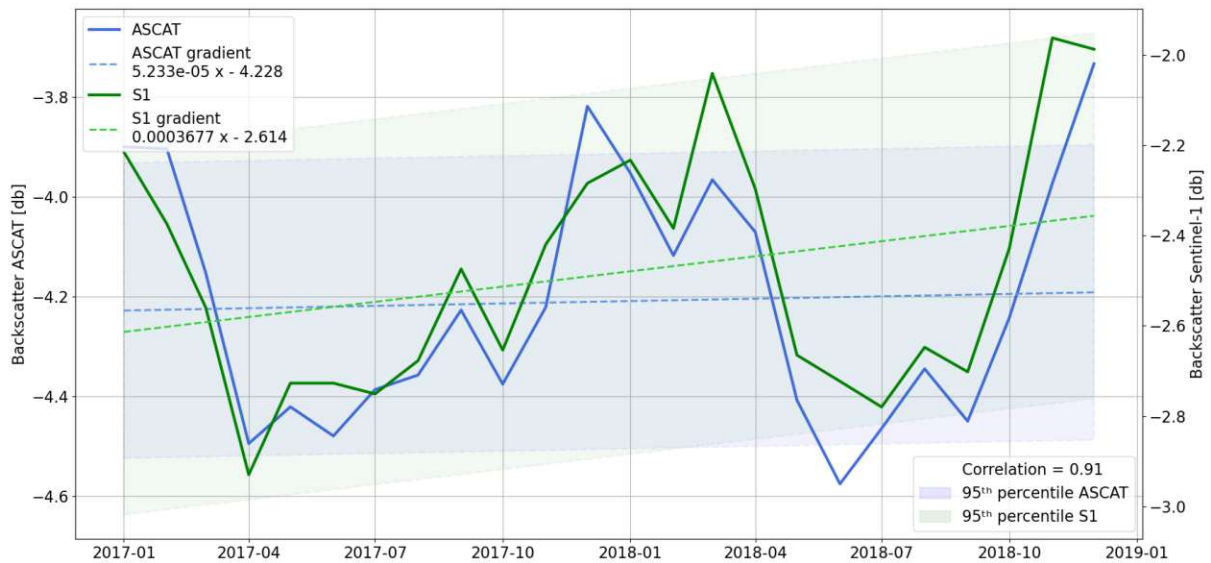
Figure 5-6. Comparison 2017 – 2019 Sentinel-1 – ASCAT monthly mean trend curves of London

5.1.4   Abu Dhabi

As depicted in Figure 3-8 the monthly means of the Abu Dhabi dataset consist of much less aggregated datapoints than the datasets of the European regions. The tile, where the 30km radius around the ASCAT midpoint is located, merely contains measurements starting from February of 2016. In the whole year of 2016 the monthly means are almost at a flat plane, showing no signs of significant changes whereas there are quite significant changes in the ASCAT trend curve during this time period present.
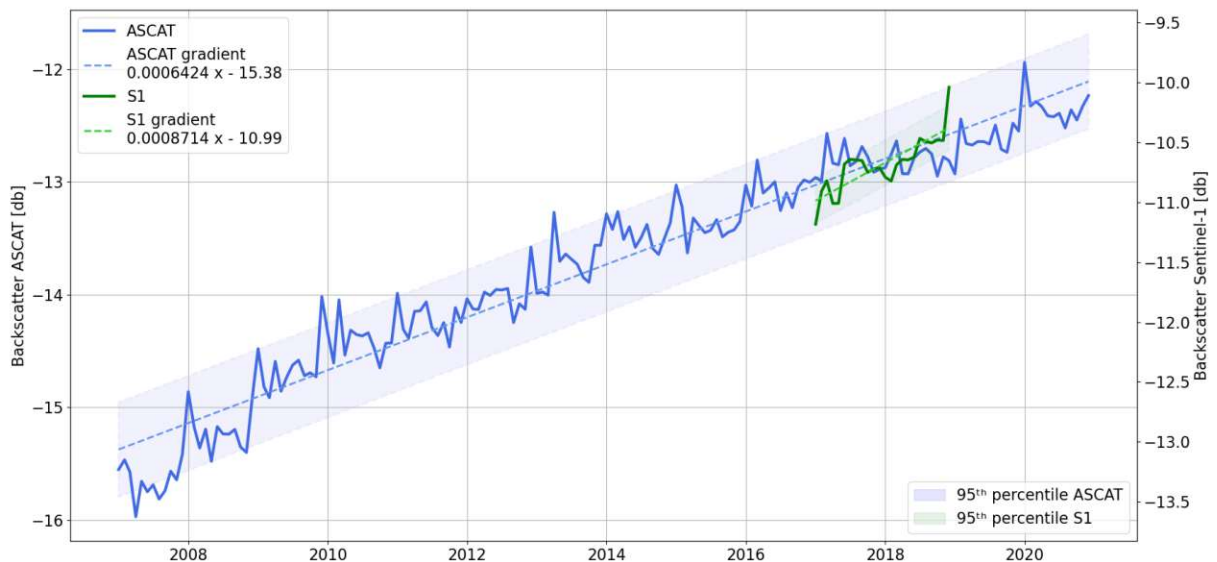
Figure 5-7. Comparison of the complete ASCAT trend with the 2017 – 2019 Sentinel-1 trend curves of Abu Dhabi

Comparing the 2017 – 2019 Sentinel-1 curve to the total ASCAT trend a large difference especially at the end and the beginning of the Sentinel-1 curve is present (see Figure 5-7).
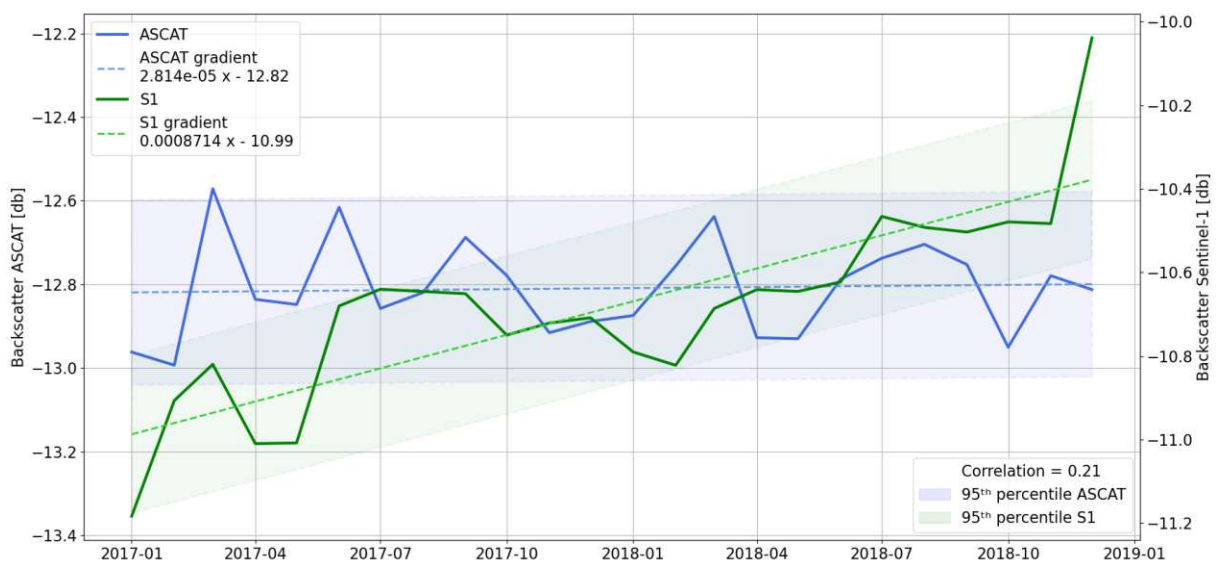
Figure 5-8. Comparison 2017 – 2019 Sentinel-1 – ASCAT monthly mean trend curves of Abu Dhabi

The detailed analysis (see Figure 5-8) shows that there is no significant correlation between the two slopes which results in the low correlation coefficient. This can be explained by the much lower amount of satellite passes and therefore fewer measurements per month.

5.1.5 Shanghai

The trends of the Shanghai region inherit the same problem as the ones of Abu Dhabi with regard to the low number of aggregated measurements. This results in an unstable behaviour, which can be seen throughout the whole time frame. The two spikes at the beginning of 2018 can be explained with the two dips in the amount of satellite passes (see Figure 3-8). During the year 2016 there are two huge spikes, one positive and one negative, present. This can be explained by the combination of low numbers of measurements and the absence of Sentinel-1B since there were no obvious abnormalities in the monthly mean data visible.
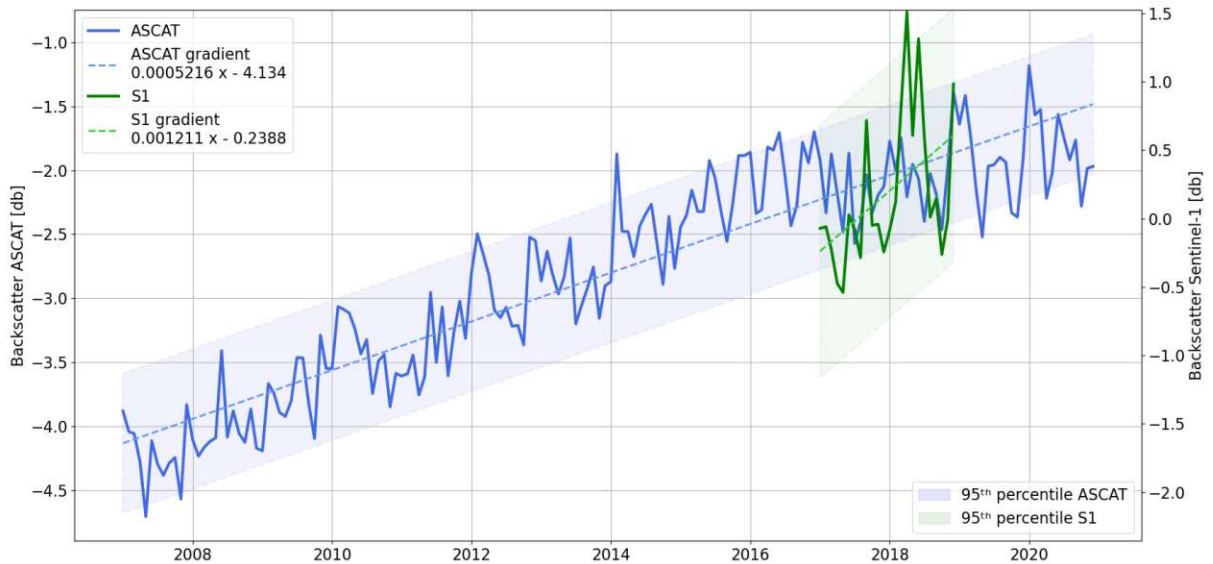
Figure 5-9. Comparison of the complete ASCAT trend with the 2017 – 2019 Sentinel-1 trend curves of Shanghai

Comparing the 2017 – 2019 Sentinel-1 trend with the complete ASCAT curve the two spikes in 2018 and the much steeper Stentinel-1 gradient are obvious (see Figure 5-9).
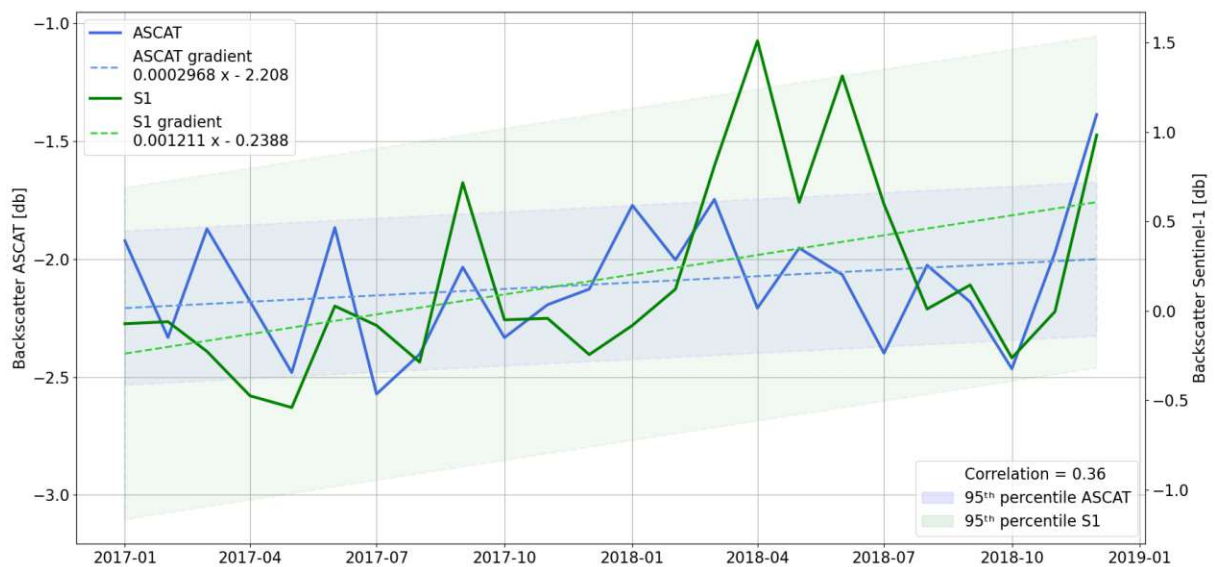
Figure 5-10. Comparison 2017 – 2019 Sentinel-1 – ASCAT monthly mean trend curves of Shanghai

Comparing the two datasets at the two-year time period the only time where they match sufficiently is at the last three months of the trend curve. Considering the behaviour of the presuming curve this match is considered rather random.

5.2 Gradient Maps

The next step was an in-depth analysis of the Sentinel-1 dataset in regards to what effects are contributing to the behavior of the trend curves. This has been done using the calculated gradient maps explained in chapter 4.4 in combination with the timelapse feature of GoogleEarth. In all datasets generally the most significant changes are located in urban environments. Positive gradients can be found mostly around newly built structures and around construction sites (see Figure 5-11). Also some areas with negative gradients can be observed because of the movements of goods. The movement of objects often results in a change of backscatter behaviour where the amplitude seems to depend on the material which the objects are made of. A very prominent example of negative gradient occurance are railroads where the removal of trains results in a drop of backscatter values (see Figure 5-12). Outside of urban areas most gradient changes occur in cropland, where the changes in vegetation as well as simple changes in farming directions have a big influence on the backscatter behaviour.
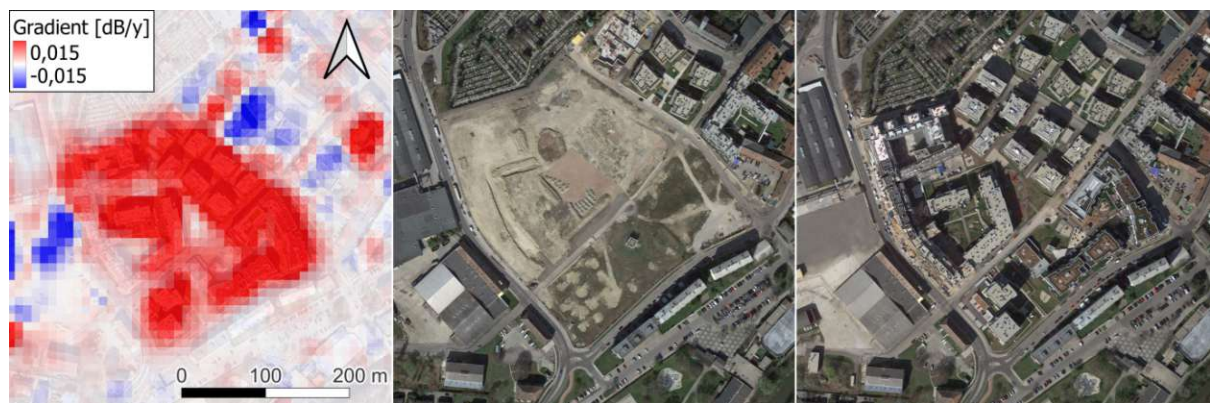
Figure 5-11. Building construction in the village of Schwechat next to Vienna, orthophotos provided by Maxar Technologies and extracted from Google Earth

The strong variations in backscatter behaviour in urban areas can be caused by a huge variety of effects and the interplay of multiple sources like buildings (height, materials and geometry), general surfaces and vehicles. Because of the difference in observation angle due to the satellite orbits and the constant movement of traffic, fluctuations in backscatter values are more present in these areas compared to grasslands and forests, where differences in observation angles have much less effect.

Figure 5-12. Impact of railways and train stations at the example of the Penzing railway station, orthophotos provided by Maxar Technologies and extracted from Google Earth

Along railroads, especially ones with multiple tracks, large negative gradient values could be observed alongside with some patches of positive gradients. This is caused by the movement of trains and can be compared to the movement of containers in an container port. The reason why the overwelming majority of the affected pixel gradients are negative could not be solved completely and is suspected to be a random effect between the movement of trains, the moment of satellite imaging and the direction of observation.

5.2.1 Gradient Map Vienna
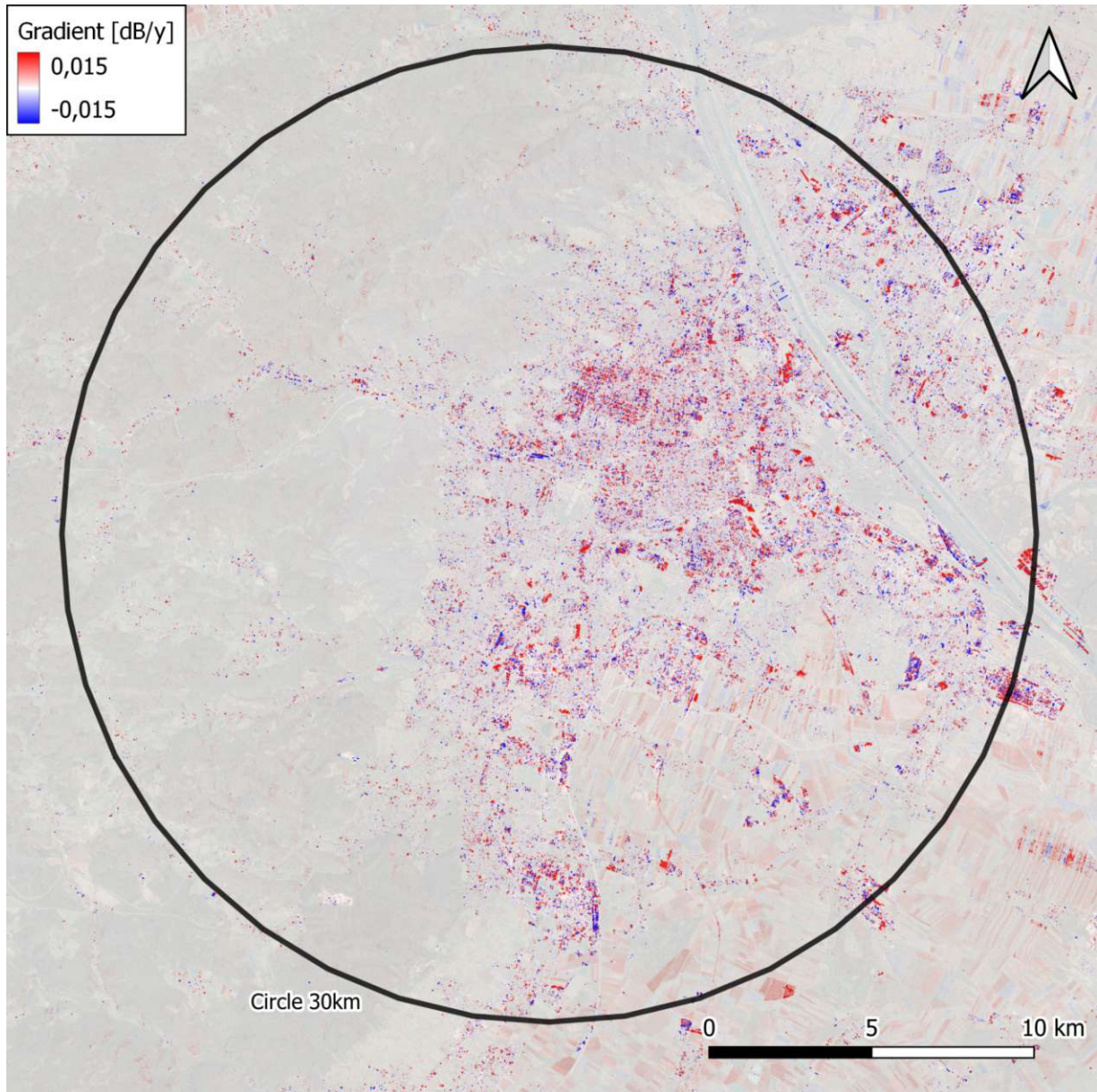
Figure 5-13. Gradient map of Vienna

In the Vienna area most changes happen in regions, where new structures have been built or existing structures have been expanded (see Figure 5-13). A prominent example is the newly built main railroad station six kilometres east of the circle centre (see Figure 5-14). In contrast, the woodland in the west is very consistent in backscatter behaviour.
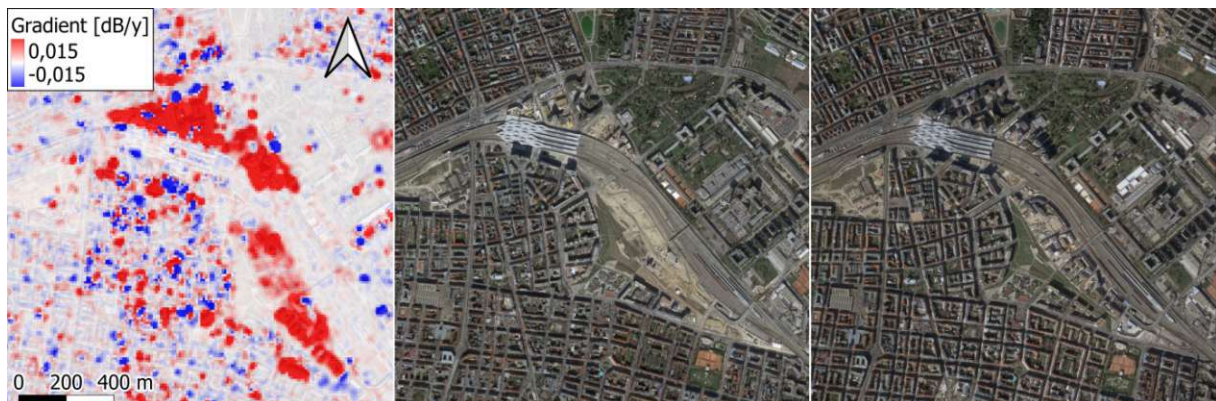
Figure 5-14. Construction site Vienna main station, orthophotos provided by Maxar Technologies and extracted from Google Earth

During the chosen time period significant construction work took place especially north and southeast of the departure hall which has been completed approximately three years earlier. All areas where new buildings have been constructed show consistent positive gradients.

Figure 5-15. OMV central storage in the east of Vienna, orthophotos provided by Maxar Technologies and extracted from Google Earth

The central oil storage of the OMV company in the east of Vienna next to the Danube shows a large quantity of positive gradients despite no visible change can be seen in the optical datasets (see Figure 5-15). The outside of the containments consist largely of curved metal sheeting which makes them an excellent reflector. Theoretically, emitted radiation from other sources could be redirected to the satellite. An increase of this radiation could lead to an increase of detected backscatter.

Figure 5-16. Container company in the south of Vienna, orthophotos provided by Maxar Technologies and extracted from Google Earth

Near areas where containers are in motion (container harbours, shipping companies...) a mixture of very low and very high gradient values can be observed. A prominent example in the Vienna region is a container company to the South of Vienna next to the highway (see Figure 5-16). This strong response is caused by the metal surface of the containers which has a much higher reflectivity than the surrounding concrete ground.

5.2.2 Gradient Map Patzmannsdorf
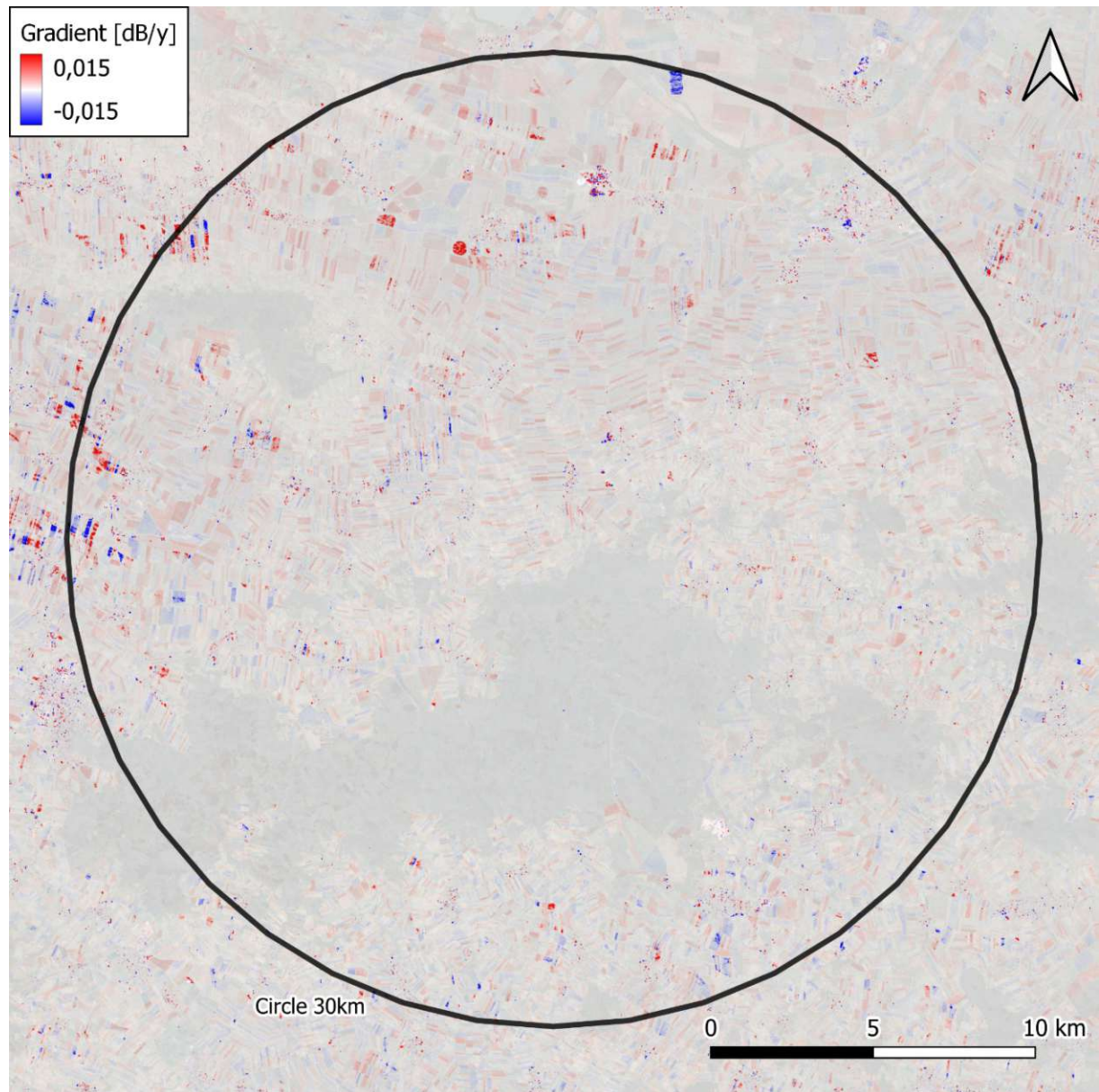
Figure 5-17. Gradient map of the Patzmannsdorf area

Contrary to the urban area datasets the rural dataset of the Patzmannsdorf region exhibits very consistent backscatter values in the examined timeframe (see Figure 5-17). Significantly positive and negative gradient values exist in the agricultural regions, where changes in crop, watering or farming directions lead to changes in backscatter (see Figure 5-18).
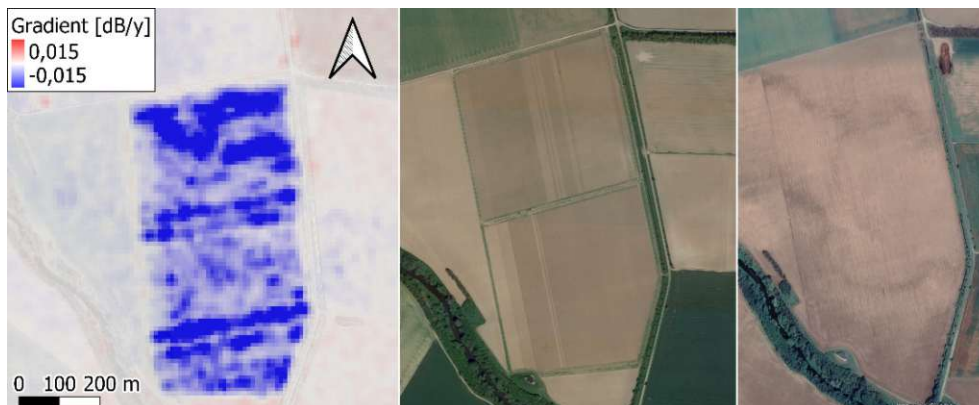
Figure 5-18. Example for the change in farming direction in the north of the region of Patzmannsdorf, orthophotos provided by Maxar Technologies and extracted from Google Earth
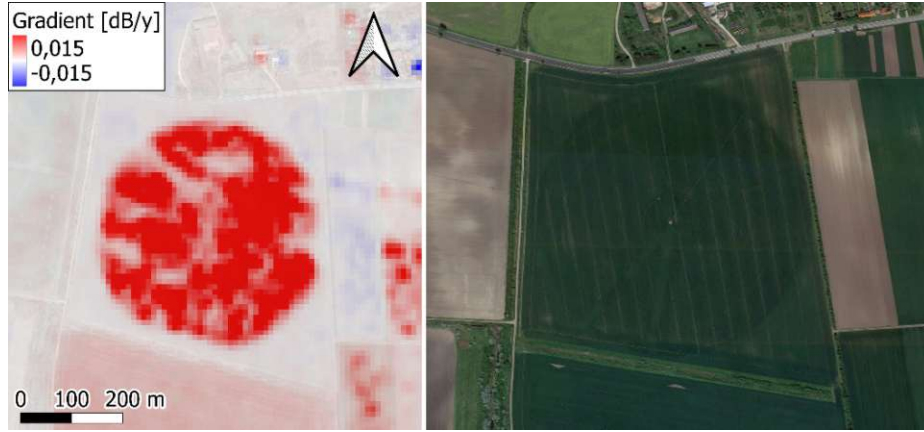
Figure 5-19. Visible circular watering pattern, orthophotos provided by Maxar Technologies and extracted from Google Earth

In the northwest of the Patzmannsdorf region a big red dot is visible which is caused by a circular structure that appears to be responsible for watering the surrounding field (see Figure 5-19). Since the structure is present and appears to be active during the whole time period an explanation for this strong response could lie in the moments of satellite imaging which favour moments of higher soil saturation near the end of the period of investigation.

5.2.3 Gradient Map London
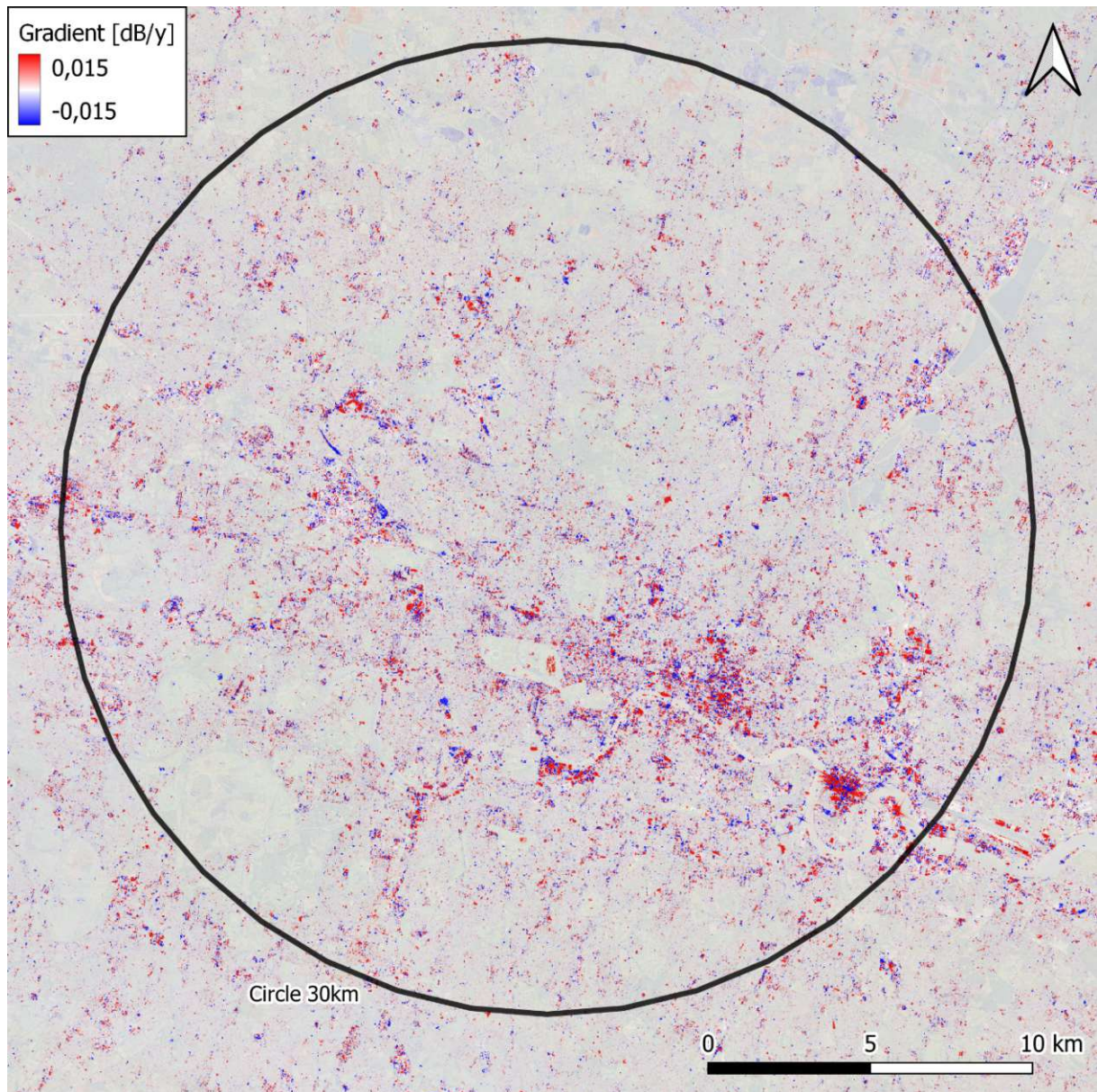
Figure 5-20. Gradient map of London

The gradient map of the London region shows large variations distributed across the whole area of interest due to the large urban share (see Figure 5-20). Near the skyscrapers located next to the river Thames double bounce effects are visible due to the combination of water and glass/metal surfaces (see Figure 5-21).
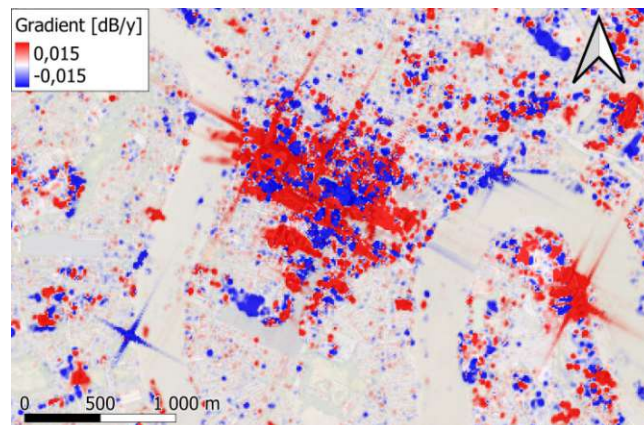
Figure 5-21. Double bounce effects Thames river

Near urban areas temporary changes of land cover play an important role. For example due to a concert in Hyde park in summer 2019 the whole grass cover has been removed and structures have been set up. The combination of new buildings and bare soil lead to a significant raise of the backscatter values in this area as can bee seen in Figure 5-22.

Figure 5-22. Concert Hyde Park, orthophotos provided by Maxar Technologies and extracted from Google Earth

5.2.4 Gradient Map Abu Dhabi
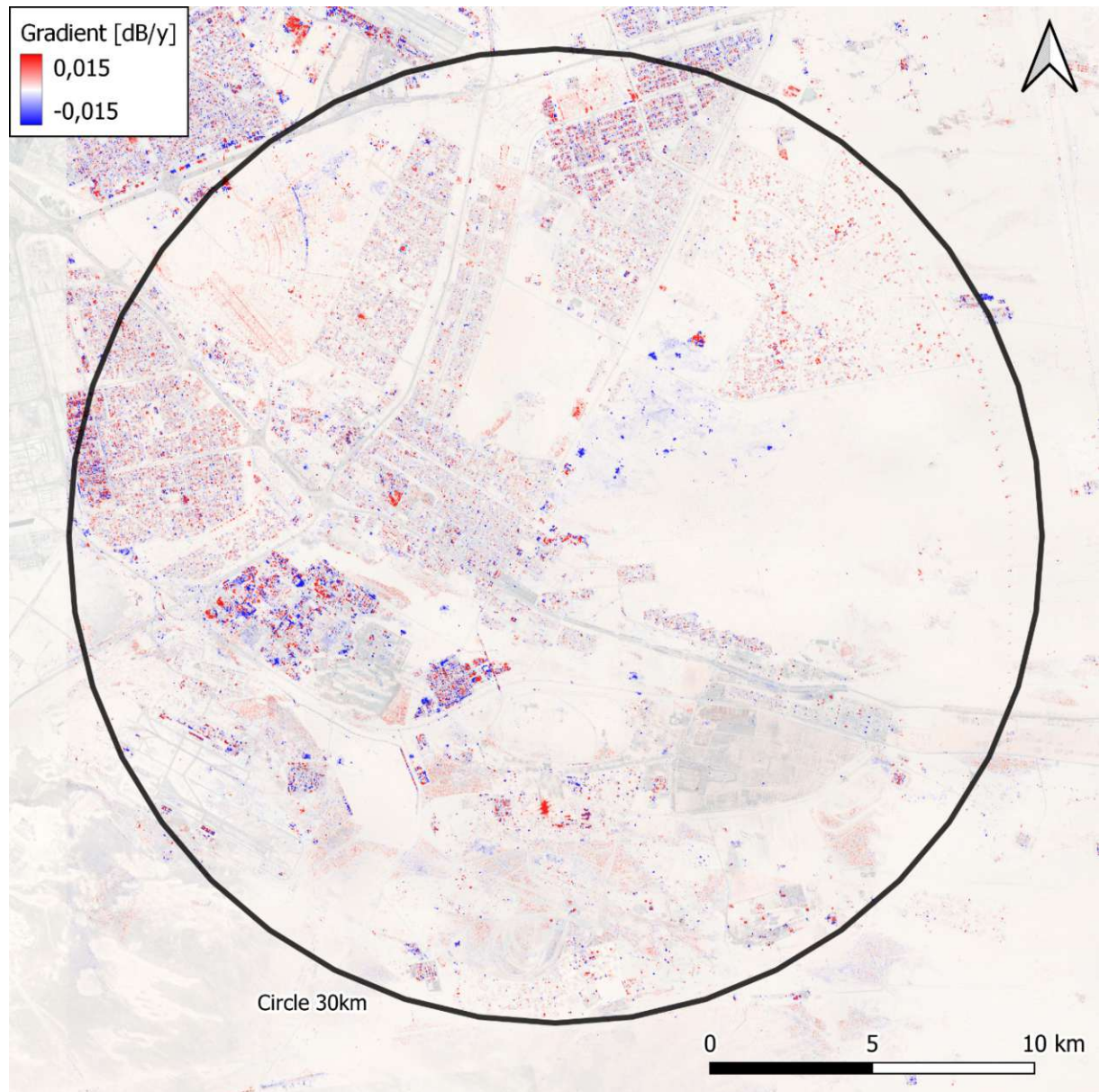
Figure 5-23. Gradient map of Abu Dhabi

The Abu Dhabi dataset shows mostly positive gradients due to newly built urban structures and negative gradients due to construction sites and the movement of goods and other manmade objects (see Figure 5-23). The almost complete lack of vegetation provides a great contrast of urban regions and the surrounding desert. Regarding the urban areas there are mostly smaller new built settlements and also some changes to existing buildings. For example there has been a change from flat roofs to angled ones in a settlement west of the midpoint (see Figure 5-24).
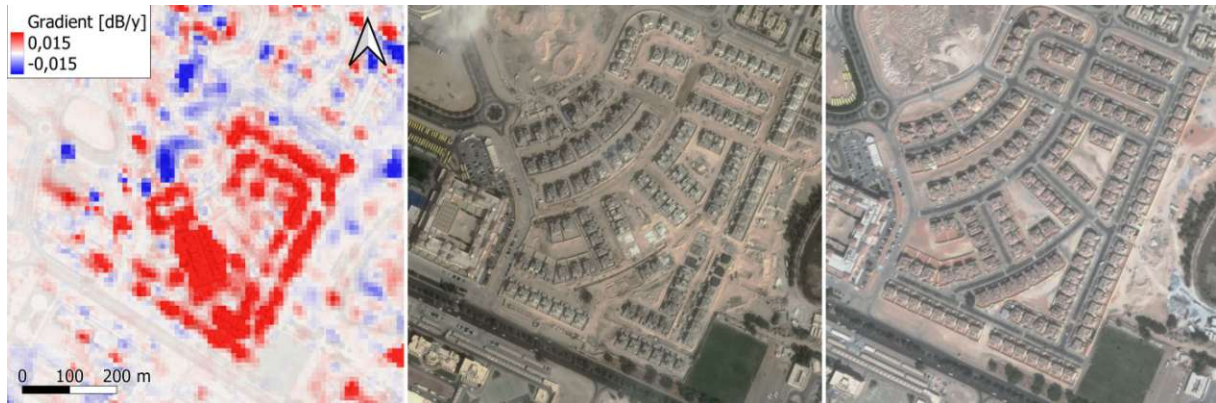
Figure 5-24. Change of roofing in suburbs of Abu Dhabi, orthophotos provided by Maxar Technologies and extracted from Google Earth

Furthermore, one area containing strong double bounce effects is present in the dataset. Comparing the optical datasets the construction of roofed structures and changes in the soil can be seen (see Figure 5-25). Because of the impact on the backscatter a combination of metal roofing and specific roof tilt angles are suspected to be the cause of the backscatter effects.
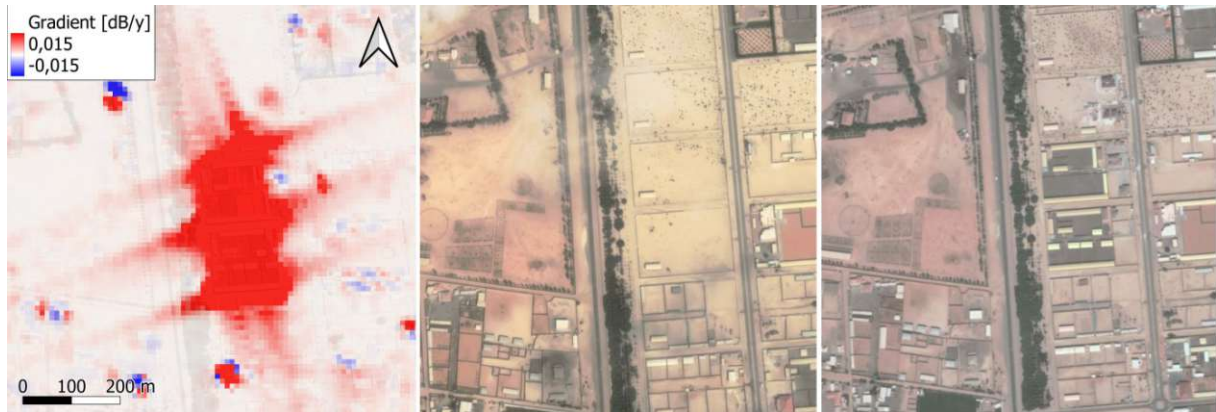
Figure 5-25. Double bounce effects because of newly built structures in Abu Dhabi, orthophotos provided by Maxar Technologies and extracted from Google Earth

5.2.5 Gradient Map Shanghai
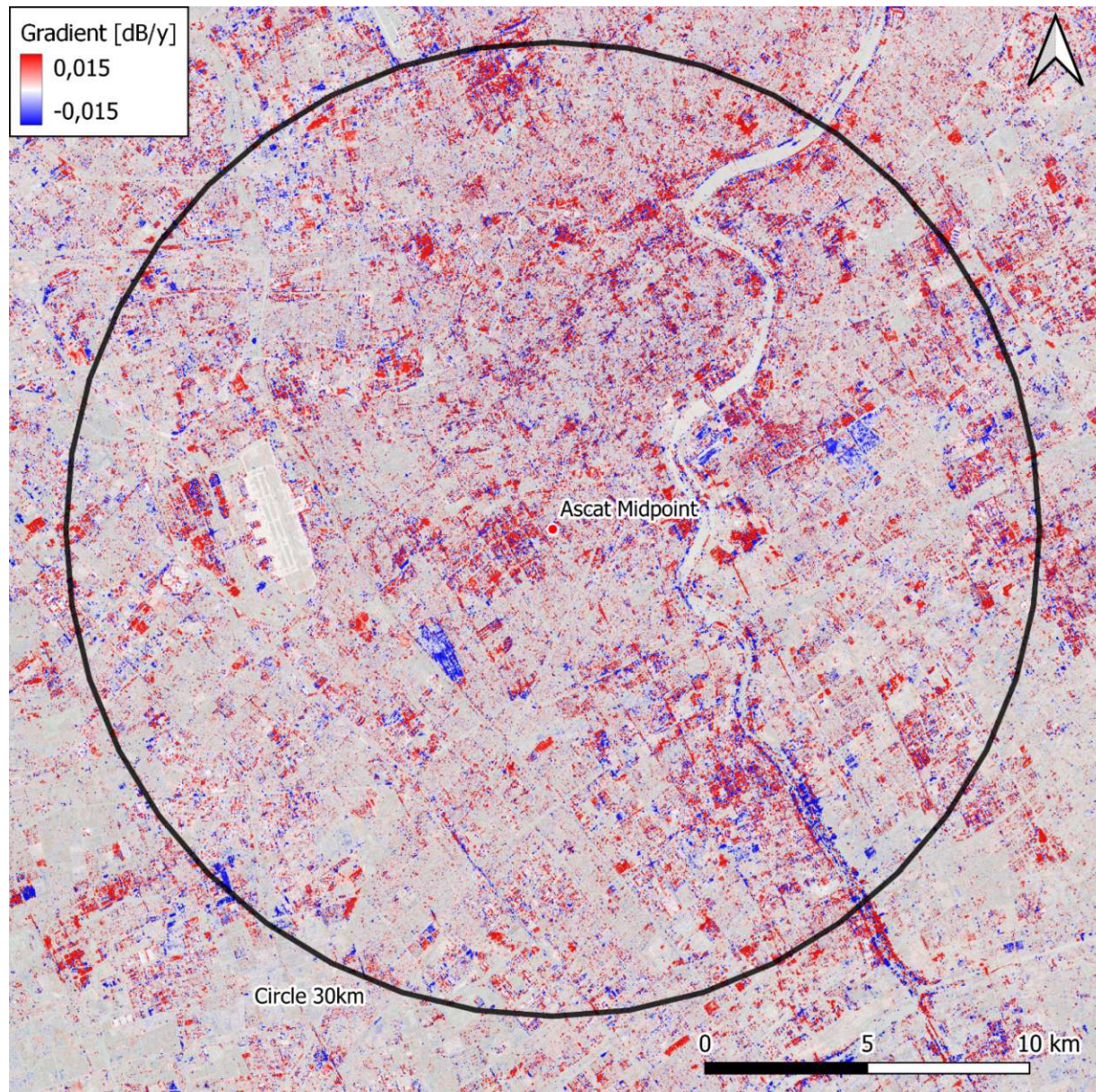
Figure 5-26. Gradient map of Shanghai

The Shanghai region has the largest deviations of gradients of all the observed areas (see Figure 5-26). This is caused by the large share of urban structures containing a large amount of skyscrapers. This type of building also leads to an accumulation of double bounce effects along the river Huangpu. Most changes in gradients are caused by the deconstruction of old structures and the building of newer ones. For example, the large blue area in the southwest is caused by the deconstruction of a large building complex in 2017 (see Figure 5-27). The former present roof structures were a much better reflector than the bare soil which was left.

Figure 5-27. Removal of buildings (01/2017 – 12/2018), orthophotos provided by Maxar Technologies and extracted from Google Earth

Scattered over the whole dataset double bounce effects are present because of the high number of skyscrapers. The very strong angle signal depicted in Figure 5-28 visualizes the antenna pattern.
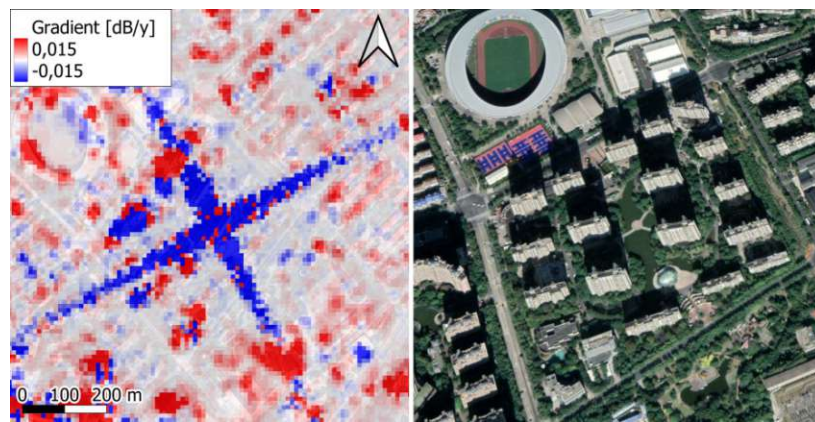
Figure 5-28. Double bounce effect between skyscrapers in Shanghai, orthophotos provided by Maxar Technologies and extracted from Google Earth

5.3 Classification Results

To pinpoint the impact of urban areas on the Sentinel-1 datasets the data has been classified using the method explained in Chapter 4.5. Because of the inconsistent trend curve behaviour of the Shanghai and Abu Dhabi datasets only the European regions were classified using the monthly-aggregated backscatter values. For each of the three masks the corresponding pixel value mean trend curves were calculated for the masked and the non-masked pixels.

5.3.1 Classification Vienna

a)   b)
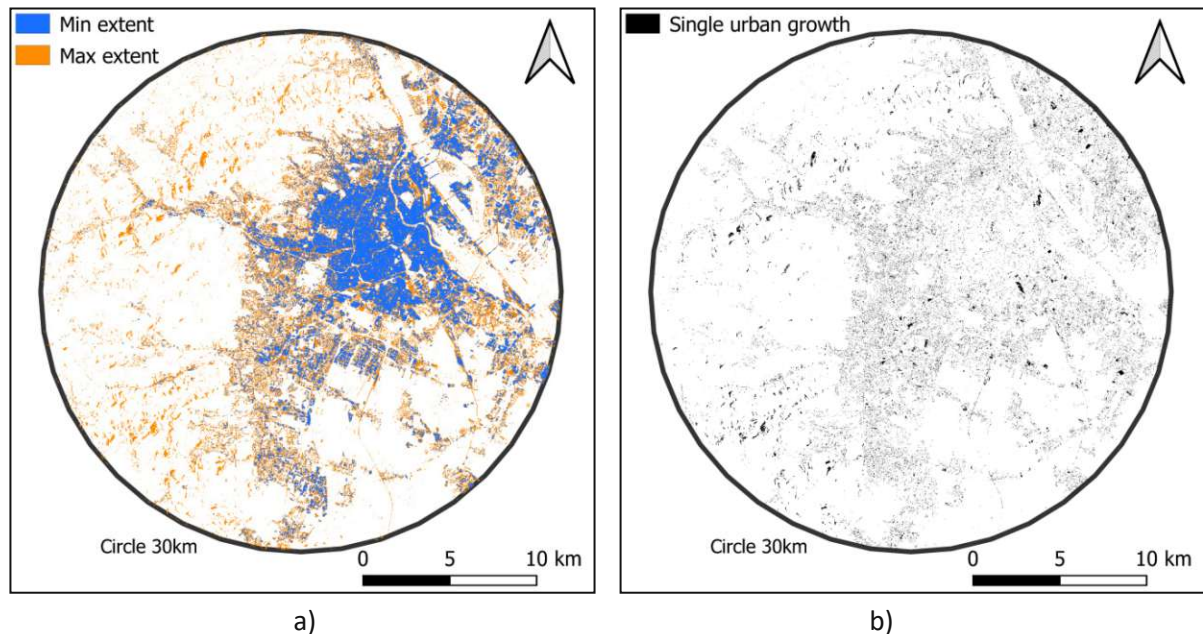
Figure 5-29. Masks Vienna: a) *Maximum* and *minimum* extent mask. b) *Single urban growth* mask.

The *maximum extent* mask shows many misclassified pixels in the western rural areas, which were mostly caused by foreshortening in the mountainous areas. The *minimum extent* mask provides a good representation of big urban regions, but falls short in classifying small villages. The *single urban growth* mask mostly highlights regions, which show positive in the gradient map. In the west there are misclassifications because of foreshortening. The *maximum extent* algorithm masked 27% of the pixels and returned a trend curve which follows the ASCAT curve quite closely (see Figure 5-30). The same can be observed by looking at the trend curve from the *minimum extent* algorithm, which masked 12% of the available pixels (see Figure 5-31).

Figure 5-30. Bias-corrected trend curve comparison – *maximum extent* mask
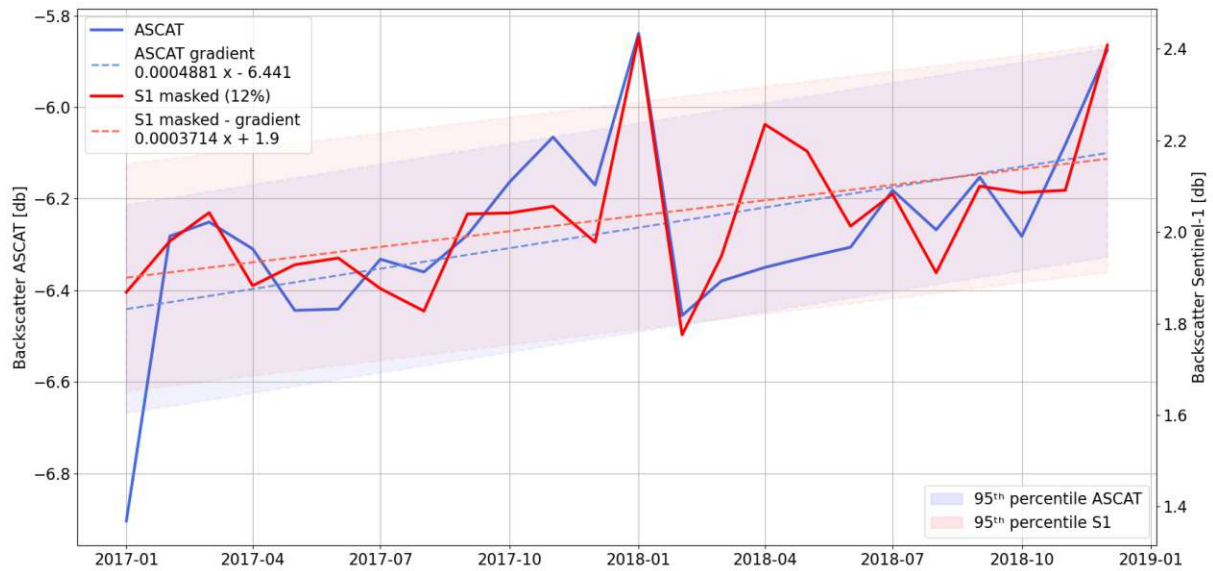
Figure 5-31. Bias-corrected trend curve comparison – *minimum extent* mask

The comparison of the *single urban growth* trend with the ASCAT trend shows that the detailed behaviour of the masked trend curve remains the same but aligns along a rising gradient (see Figure 5-32). This is suspected to happen because of the nature of the algorithm.
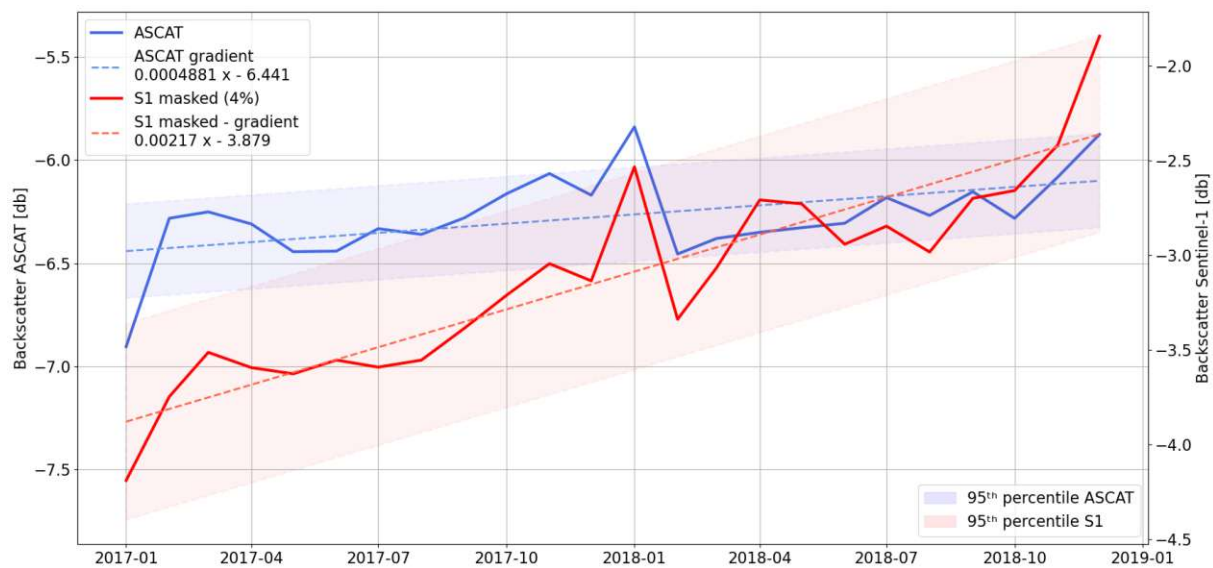
Figure 5-32. Bias-corrected trend curve comparison – *single urban growth* mask

5.3.2 Classification Patzmannsdorf
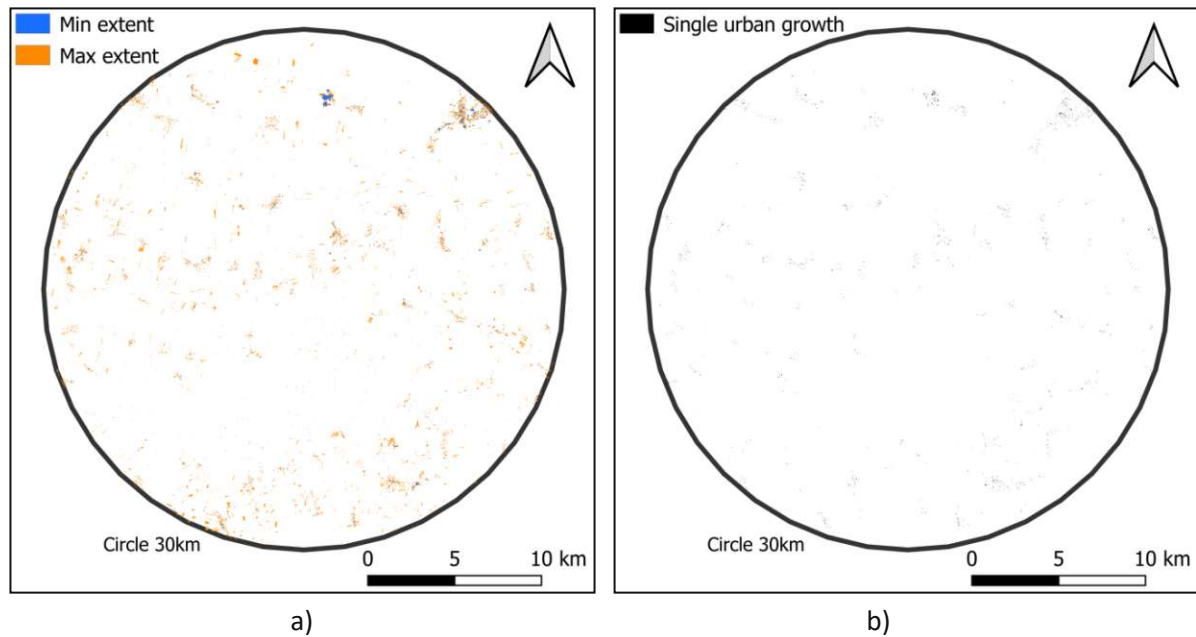
Figure 5-33. Patzmannsdorf: a) *Maximum* and *minimum extent* mask. b) *single urban growth* mask.

In the Patzmannsdorf region all algorithms mask really small percentages of the available pixels. This is caused by the lack of urban structures and therefore the lower backscatter values, which are mostly below the thresholds. This results in 2% masked pixels of the *maximum extent*, 0.2% masked pixels of the *minimum extent* and 0.1% masked pixels of the *single urban growth* algorithm. Because of these low percentages the trend curves provide little to no information regarding their impact on the complete Sentinel-1 trend of Patzmannsdorf and are left out.

5.3.3 Classification London
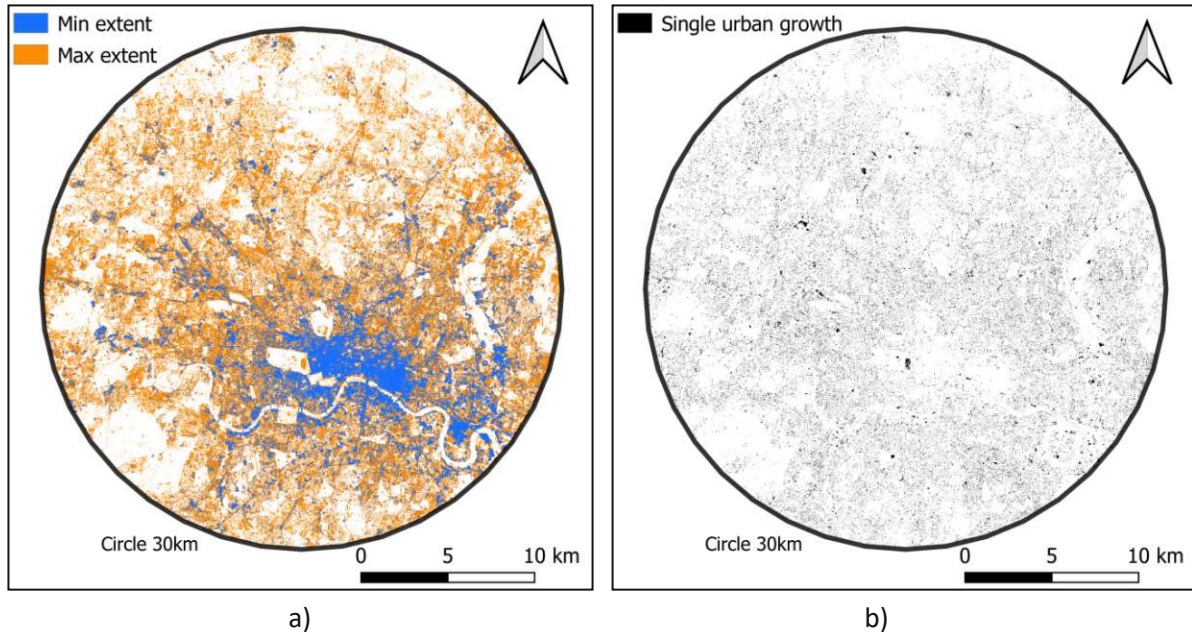
Figure 5-34. London: a) *Maximum* and *minimum* extent masks. b) *Single urban growth* mask.

The *maximum extent* algorithm masks 48% of the available pixels from the heavily urbanized area of London. The *minimum extent* algorithm masks 13% of the pixels whereas the *single urban growth* algorithm returns 6% of the total pixels.

Figure 5-35. Bias-corrected trend curve comparison – *maximum extent* mask

The *maximum extent* (Figure 5-35) and the *minimum extent* (Figure 5-36) algorithm trend curves of London are very similar despite the difference in the number of masked pixels. The trend curves also match the complete trend curve (Figure 5-6) very well.

Figure 5-36. Bias-corrected trend curve comparison – *minimum extent mask*

The *single urban growth* algorithm returns a trend curve which behaves similarly to the one of the Vienna region.
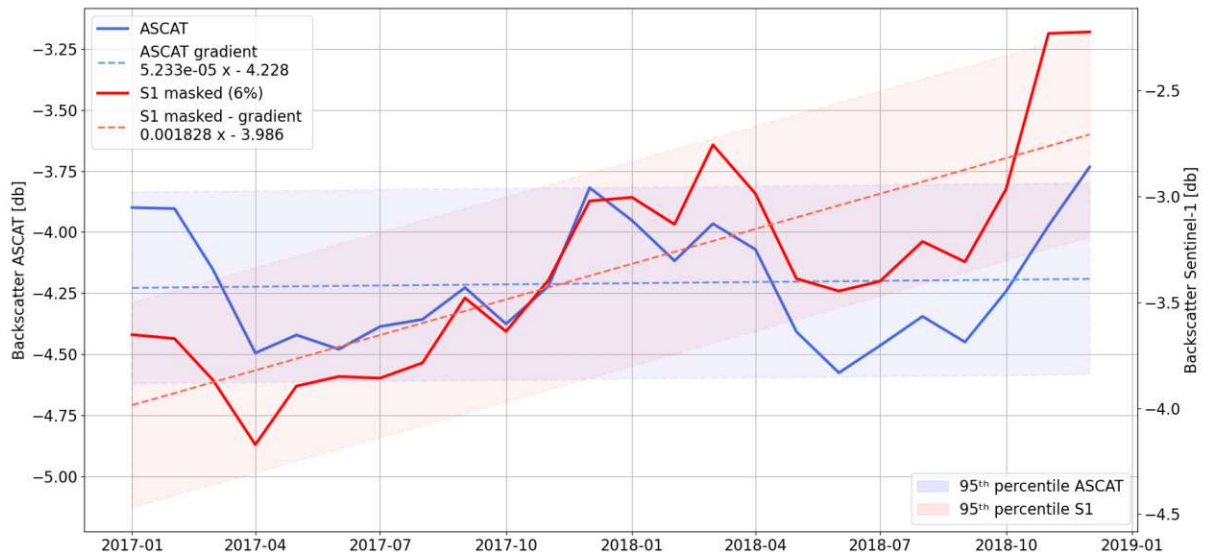
Figure 5-37. Bias-corrected trend curve comparison – single urban growth mask

5.3.4   Classification Summary

For each city region the *maximum extent* and the *minimum extent* trends are very similar with the interesting difference, that the gradient slopes of the *maximum extent* trends are slightly steeper. The *single urban growth* classification returns small percentages of pixels as classified, which can be explained by the large time period of investigation, where there is high probability for the pixels to be ruled out by the algorithm. Therefore, it mostly recognizes areas, where large changes in backscatter behaviour happened in a short time period. The Patzmannsdorf region shows very small classification percentages because of the small amount of urban areas in the region. The results confirm that the algorithm works as expected and it is for example not influenced by changes in agriculture.

Table 5-1. Comparison of mean trend curve gradients between masked and non-masked data

Gradient (masked/ non-masked)	Vienna [dB/y]	Patzmannsdorf [dB/y]	London [dB/y]
Maximum Extent	0.1/0.3 (27%/73%)	0.1/0.4 (2%/98%)	0.15/0.1 (48%/52%)
Minimum Extent	0.1/0.3 (12%/88%)	-0.05/0.4 (0.2%/99.8%)	0.15/0.1 (13%/87%)
Single Urban Growth	0.8/0.15 (4%/96%)	0.7/0.4 (0.1%/99.9%)	0.7/0.1 (6%/94%)
S1 2017-2019	0.2	0.4	0.15
ASCAT 2017-2019	0.15	0.4	0.02
ASCAT 2007-2021	0.06	0.016	0.05

Comparing the results in Table 5-1 following significant behaviours can be pointed out:

- In Vienna and Patzmannsdorf the *maximum* and *minimum extent* masked pixels have a much smaller gradient than the non-masked pixels. In London this behaviour is present in the opposite way (but not as significant).

- The *single urban growth* algorithm provides almost the same gradient behaviour in the two city regions whereas in the Patzmannsdorf region the difference between masked and non-masked is much smaller.

- Urbanisation seems to lead to a flatter gradient and a higher backscatter signal level.

6 Summary, Conclusion and Outlook

Urban areas have distinctive microwave backscatter characteristics, which differ greatly from naturally occurring types of land cover. Visible trends in datasets from urban areas like the ASCAT backscatter suggest that the growth of urban land cover could be one of the major reasons behind this behaviour. Previous studies show that different sensor systems, operating in the optical or microwave domain, are very capable in detecting all kinds of differences regarding urban structures and their temporal behaviour.

The ASCAT datasets have low resolution but show distinctive trends in the urban areas whereas the chosen Sentinel-1 datasets provide high spatial and temporal resolution, which is needed for the fine-scale investigations. After applying the same temporal and spatial resolution the correlation between the ASCAT datasets and the Sentinel-1 datasets of the European regions is remarkably high. The datasets of the Shanghai and Abu Dhabi regions lack a significant correlation, which is presumably caused by the low amount of Sentinel-1 measurements, which results in erratic Sentinel-1 trend curves.

The derived gradient maps make use of the high resolution provided by the Sentinel-1 datasets and highlight areas, which are subject to backscatter changes. These fine-scale maps make it possible to distinguish different backscatter behaviour caused by urban structures. Even in the regions of Shanghai and Abu Dhabi the gradient maps provide useful information after adjusting the scale to cope with the very narrow (Abu Dhabi) or very wide (Shanghai) spread of gradient data.

Masking the European datasets with simple threshold based algorithms allows the isolation of urban areas and areas which inherit urban growth. The steeper gradient slope of the *maximum extent* algorithms could be caused by the amount of not fully urbanized pixels compared to the almost complete urbanized pixels of the *minimum extent* algorithms. Therefore, the trends of the *maximum extent* algorithm are more affected by the effects of urban growth. The results of the *single urban growth* algorithms lead to the conclusion that one reason for a rise in backscatter signal strength is the switch from non-urban to urban environment but the chosen function lead to a very small number of classified pixels.

The different used methods highlighted, that there are many small-scale effects, which affect the radar backscatter behaviour. The expansion of urban areas, the transition from older style buildings to modern architecture, containing more and more metal and glass surfaces and the continuous sealing of soil contribute heavily in the rise of radar backscatter. Isolating the sole effects of urban growth proved to be very difficult because of the vast amount of various contributing mechanisms. By analyzing the masked datasets it was possible to get a rough estimation of the impact of the urban pixels on the complete trend.

In conclusion the human impact on the datasets is visible in all results and it is possible to extract some parts of urban growth using the high resolution datasets provided by the Sentinel-1 satellite system. It is also possible to correlate the Sentinel-1 datasets with the ASCAT datasets as long as there are sufficient numbers of measurements and complete, undistorted datasets. Specific quantification of the impact from isolated urban growth on the ASCAT trend could not be achieved with the used algorithms. The present thesis shows that the Sentinel-1 dataset provides the quality to isolate specific effects on the temporal behaviour of backscatter. This leads to the conclusion that, together with second data sources like land cover data or optical datasets, it should be possible to isolate areas which are mainly affected by urban growth. The better the classification of urban areas gets, the easier a quantification of its behaviour and therefore the creation of a mathematical model for its correction should be.

Image Index

List of Tables

Bibliography

[1] F. T. Ulaby, R. K. Moore and A. K. Fung, "Microwave remote sensing - Active and passive.," Norwood, MA, Artech House, 1982.

[2] Y. Dong, B. Forster and C. Ticehurst, "Radar backscatter analysis for urban environments," *International Journal of Remote Sensing, vol. 18, no. 6.,* pp. 1351-1364, April 1997. doi: 10.1080/014311697218467.

[3] D. Clark, Urban Geography (Routledge Revivals), London: Routledge, 1982. doi: 10.4324/9780203796641.

[4] B. Bhatta, "Analysis of Urban Growth and Sprawl from Remote Sensing Data," Kolkata, India, Springer-Verlag Berlin Heidelberg, 2010. doi:10.1007/978-3-642-05299-6.

[5] S. Frolking, T. Milliman, R. Mahtta, A. Paget, D. G. Long and K. C. Seto, "A global urban microwave backscatter time series data set for 1993–2020 using ERS, QuikSCAT, and ASCAT data," *Scientific Data, vol. 9, no. 1. Springer Science and Business Media LLC,* 16 March 2022. doi: 10.1038/s41597-022-01193-w..

[6] Stadt Wien, "wien.gv.at," 01 01 2022. [Online]. Available: https://www.wien.gv.at/statistik/lebensraum/tabellen/nutzungsklassen-bez.html.

[7] Stadt Wien, "wien.gv.at," 01 01 2022. [Online]. Available: https://www.wien.gv.at/statistik/bevoelkerung/bevoelkerungsstand/.

[8] Eurostat, "ec.europa.eu," 01 01 2022. [Online]. Available: https://ec.europa.eu/eurostat/data/database.

[9] UN, "population.un.org/," 01 01 2022. [Online]. Available: https://population.un.org/wpp/.

[10] "Statistik.at," 01 01 2022. [Online]. Available: https://www.statistik.at/web_de/klassifikationen/regionale_gliederungen/ortschaften/index.html .

[11] EUMETSAT, "ASCAT User Guide," Darmstadt, 2017.

[12] "ESA," 01 01 2022. [Online]. Available: https://sentinel.esa.int/web/sentinel/missions/sentinel-1/satellite-description.

[13] R. Torres, P. Snoeij, D. Geudtner, D. Biddy, M. Davidson, E. Attema, P. Potin, B. Rommen, N. Floury, M. Brown, I. Navas-Traver, P. Deghaye, B. Duesmann, B. Rosich, N. Miranda, C. Bruno, M. L'Abbate, R. Croci, A. Pietropaolo, M. Huchler and F. Rostan, ""GMES Sentinel-1 Mission", "The Sentinel Missions – New Opportunities for Science"," *Special Issue of Journal of Remote Sensing of Environmen, Vol 120,* pp. 9-24, May 2012.

[14] CGLOPS-1, "Copernicus Global Land Operations - MODERATE DYNAMIC LAND COVER COLLECTION 100m," Global, 2015.

[15] S. Hahn, W. Wagner, S. C. Steele-Dunne, M. Vreugdenhil and T. Melzer, "Improving ASCAT Soil Moisture Retrievals With an Enhanced Spatially Variable Vegetation Parameterization," *IEEE Transactions on Geoscience and Remote Sensing, vol. 59, no. 10,* pp. 8241-8256, October 2021, doi: 10.1109/TGRS.2020.3041340..

[16] V. Naeimi, S. Elefante, S. Cao, W. Wagner, A. Dostalova and B. Bauer-Marschallinger, "Geophysical Parameters Retrieval from Sentinel-1 SAR Data: A Case Study For High Performance Computing At EODC.," 24th High Performance Computing Symposium, 2016. doi: 10.22360/springsim.2016.hpc.026.